

The turbulent flow within a wind-aligned street canyon with trees: an experimental study

Annika Vittoria Del Ponte^{1,2} · Sofia
Fellini¹ · Massimo Marro² · Lionel
Soulhac² · Luca Ridolfi¹ · Pietro
Salizzoni^{1,2}

Received: DD Month YEAR / Accepted: DD Month YEAR

Abstract

Most studies on the aerodynamic impact of trees on street canyon ventilation focus on external winds perpendicular to the street axis, as these are crucial for dispersing ground-level pollutants like vehicle emissions. Other wind directions, despite their importance for urban pollutant dispersion, receive less attention. Non-perpendicular winds introduce an advective component along the canyon, which is strongly influenced by tree presence and density, significantly shaping pollutant spread across downwind streets. To address this gap, we conducted velocity measurements in a reduced-scale street canyon aligned with the external flow, varying the canyon's height-to-width ratio and tree density. The aerodynamic effects of trees were simulated by placing plastic tree miniatures along the canyon's lateral walls. Our results show that trees within a square canyon reduce the mean velocity by 80% and decrease velocity fluctuations by 15% compared to an empty canyon. At the rooftop, the interaction between the external flow and tree crowns leads to a 30% increase in velocity fluctuations. As the aspect ratio decreases (i.e., for wider canyons), a vegetation-free corridor between the rows of trees results in a 25% decrease in mean longitudinal velocity and a 30% increase in velocity fluctuations compared to the empty large canyon. This induces a street ventilation more efficient with respect to the vegetated square canyon, especially when pollutants are emitted at pedestrian level. This study provides valuable experimental data for evaluating the spatially-averaged mean longitudinal velocity

¹Department of Environmental, Land, and Infrastructure Engineering, Politecnico di Torino
Corso Duca degli Abruzzi 24, 10129 Turin, Italy
Tel.: +39 011 090 7602
Fax: +39 011 090 7602
E-mail: annika.delponte@polito.it

²École Centrale de Lyon, CNRS, Université Claude Bernard Lyon 1, INSA Lyon, LMFA, UMR5509
69130, Ecully, France

in urban canyons, which can be incorporated into analytical and numerical models for better urban air quality management.

Keywords Street canyon · Trees · Turbulent flow field · Wind direction · Wind-Tunnel experiments

1 Introduction

Trees are a common green infrastructure adopted to improve the thermal comfort in the urban environment (Jia and Wang 2021). The presence of trees within street canyons decreases air temperature by shading and increases moisture by transpiration (Aboelata and Sodoudi 2020; Segura et al. 2022; Wang et al. 2024). Moreover, trees promote the deposition of both gaseous and particle pollutants with an efficiency which depends on the leaf area density, wind speed, and plant species (Beckett et al. 2000; Zhang et al. 2021; Linden et al. 2023).

However, the aerodynamic impact of trees on air quality is not always beneficial, as it can inhibit ventilation within street canyons — an aspect that must be considered when designing green infrastructure (Tomson et al. 2021). Several experimental studies have evaluated the aerodynamic impact of trees on airflow and pollutant concentration within canyons perpendicular to the prevailing wind, a scenario considered the most detrimental to air quality. Pioneering experimental studies by Gromke and Ruck (2007, 2009) demonstrated that trees with large crowns, or small tree spacing, cause an increase in the mean scalar concentration in the canyon higher than smaller or scattered trees, and that the concentration of pollutants (emitted at ground level) is sensitive to variation in crown porosity after a threshold of 97%. More recently, Fellini et al. (2022) performed an experimental campaign to provide a high-resolution three-dimensional characterization of the mean concentration field within a canyon placed in an urban district for different vegetation densities. They found that, in a canyon with height-to-width ratio 0.5, the longitudinal tree spacing has a remarkable impact on the spatial distribution of the mean and turbulent pollutant concentration and that the presence of trees deteriorates the air quality at the pedestrian level. Conversely, smaller vegetation (i.e., hedges) reduces the pedestrian exposure to high scalar concentration close to the canyon walls (Carlo et al. 2024). In addition to the concentration field, a few experimental studies investigated the effect of trees on the turbulent flow within street canyons. For example, Zhao et al. (2023b) found that large trees dampen momentum fluxes at the canyon rooftop and hinder heat removal from the inner canyon to the rooftop, while small trees enhance turbulent fluctuations and promote airflow exchange with the external flow. Recently, Del Ponte et al. (2024) exploited simultaneous measurements of velocity and scalar concentration, to investigate the influence of tree density on the turbulent mass fluxes inside a tree-lined street canyon. This experimental study revealed that high vegetation density significantly reduces downward turbulent mass fluxes at height of the tree canopy, leading to a reduction of the

turbulent mixing and a heterogeneous spatial pattern of the turbulent scalar field.

While numerous studies have been conducted on perpendicular street canyons, the case of canyons aligned with the wind direction has received limited attention, especially in experimental research, despite its relevance for modeling pollutant dispersion in urban environments. Assessing advective transport along the street axis is crucial, as it governs the longitudinal dispersion of pollutants (and, more generally, passive scalars) within urban canyons and influences pollutant spreading across street networks (Soulhac et al. 2013; Salem et al. 2015; Fellini et al. 2021). Previous studies (Soulhac and Salizzoni 2010; Huang et al. 2019) have shown that, in the absence of vegetation, for sufficiently long streets, a wind direction parallel to the street axis can lead to pedestrian-level pollutant concentrations that may exceed those observed in perpendicular canyons. The presence of trees further complicates dispersion dynamics by altering both mean flow structures and turbulence characteristics, thereby affecting pollutant transport mechanisms.

To our knowledge, only Gromke and Ruck (2012) conducted wind tunnel experiments within vegetated urban canyons under non-orthogonal wind directions. Their study analysed the mean concentration field in an isolated canyon with trees oriented at 0° , 45° , and 90° relative to the wind direction. The results revealed that, in canyons with trees and a low height-to-width ratio, a wind parallel to the canyon axis produced the lowest concentration levels among all tested wind orientations. The scarcity of experimental studies on vegetated street canyons aligned with the wind direction, in contrast to the abundance of studies on perpendicular configurations, highlights the need to deepen our understanding of the aerodynamics of the former through wind tunnel experiments. Such an experimental approach allows for a quantitative characterization of the phenomenon and provides valuable data to validate the numerous numerical simulations that have been conducted on this configuration (Buccolieri et al. 2011; Jeanjean et al. 2015, 2017; Maison et al. 2022). Furthermore, these experimental measurements not only support model validation but also enhance our understanding of urban canyon ventilation mechanisms, which can be parameterized in analytical models (Soulhac et al. 2008) of the flow, needed to simulate pollutant dispersion at the district scale (Soulhac et al. 2013).

To address this knowledge gap, we present results from a wind-tunnel experimental campaign aimed at examining how the presence of vegetation influences the mean and turbulent flow fields within a canyon aligned with the external wind direction. We model a two-dimensional street canyon with close lateral boundaries and two different geometries: a narrow canyon, with height-to-width ratio equal to 1, and a large canyon, with height-to-width ratio equal to 0.5. These geometries permitted the investigation of different transversal vegetation covers and the comparison of the experimental results with the analytical model by Soulhac et al. (2008). Section 2 provides a detailed description of the experimental setup and measurement techniques. In Sect. 3, we provide a detailed characterization of the boundary layer developed in the wind

tunnel. The mean and turbulent velocity fields in the canyon are described in Sect. 4, considering two different canyon geometries, notably, a square canyon (Sect. 4.1) and a large canyon (Sect. 4.2). Finally, in Sect. 5.1, we compare the experimental data with the analytical model developed by Soulhac et al. (2008), characterizing the mean flow along the longitudinal axis of a wind-aligned street canyon. In Sect. 5.2, we provide an estimate of the pressure loss coefficient associated with trees in the vegetated canyons, for varying canyon geometries. Conclusions are drawn in Sect. 6.

2 Methodology

2.1 Wind tunnel

Experiments were conducted in the atmospheric wind tunnel at the Laboratoire de Mécanique des Fluides et d'Acoustique, École Centrale de Lyon. This recirculating wind tunnel features a test section that is 12 m long, 2 m high, and 3.5 m wide. It is equipped with an axial fan capable of generating wind velocities ranging from 0.5 to 6 ms⁻¹, as well as a heat exchanger system to regulate air temperature. Inside the test section, we recreated a regular network of square streets at a 1:200 scale (see figure 1a), covering the floor with square blocks measuring 0.5 m on each side, 0.1 m high, and spaced 0.1 m apart. This setup replicates a geometry similar to that studied by Garbero et al. 2010. The combination of 0.5 m high Irwin spires (positioned at the entrance of the test section and raised 0.1 m above the floor) and small floor-mounted blocks (Irwin 1981) generates a neutrally stratified boundary layer with a thickness of $\delta = 0.9$ m and a free-stream velocity of 5 ms⁻¹. To accelerate the development of the boundary layer, the blocks were covered with 5 mm steel nuts (see also Fellini et al. 2022 and Del Ponte et al. 2024).

Within the street network, we selected a longitudinal street canyon with a length of $L = 3.5$ m and a height of $H = 0.1$ m as the reference canyon (see the yellow area in figure 1a). The lateral edges of the reference canyon were confined to simulate an infinitely long two-dimensional canyon (i.e., with a length-to-height ratio of $L/H = 35$) and to prevent disturbances in the longitudinal flow due to transversal fluxes. Two different canyon widths (W) were considered: 0.1 m and 0.2 m, creating a square canyon and a wider canyon, with height-to-width ratios (H/W) of 1 and 0.5, respectively. Note that only the reference canyon width was modified, while the rest of the network was kept with an aspect ratio H/W equal to 1. The reference canyon begins approximately 7 m from the entrance of the test section (14 times the height of the vortex generators) to ensure the flow is fully developed (Salizzoni et al. 2008). The longitudinal homogeneity of the flow along the square and the large canyons and the absence of flow perturbation due to the change in the aspect ratio are discussed in Sect. 3.2. We defined the origin of the coordinate system on the longitudinal axis of the canyon, $15H$ far from the entrance of the reference canyon, with the vertical axis starting at ground level. The x -, y -,

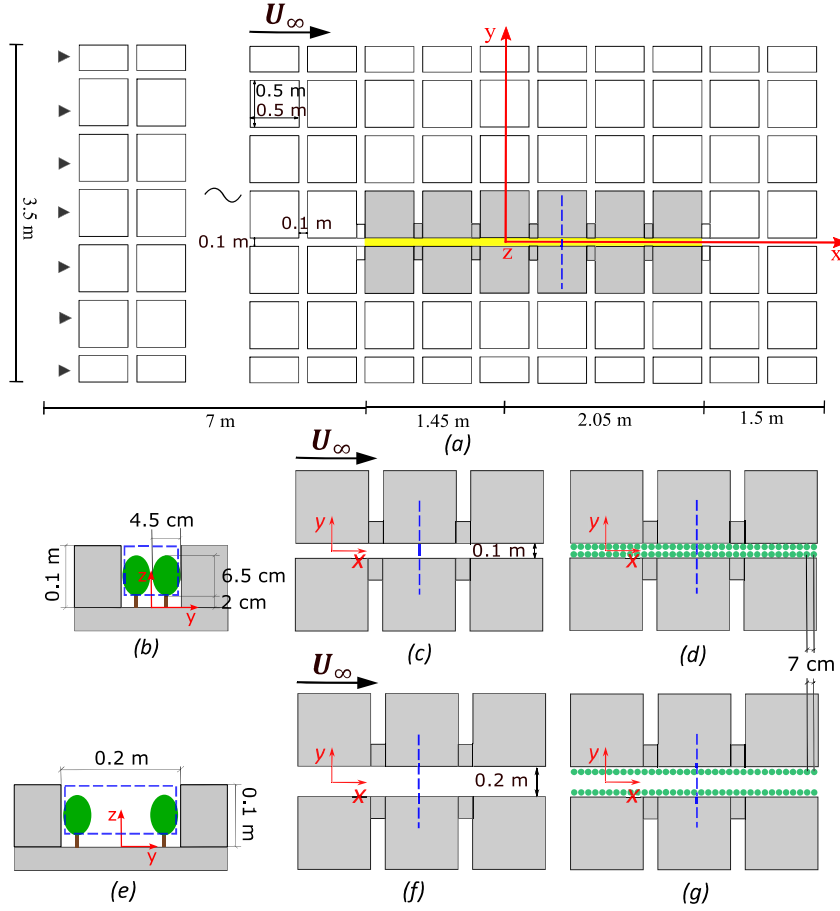


Fig. 1 (a) Scheme of the urban canopy modeled in the wind tunnel. The black triangles indicate the Irwin spires at the entrance of the test section, the red arrows represent the reference system, the yellow line marks the reference canyon, and the blue dashed line indicates the longitudinal position of the measuring section. The blocks confining the reference canyon are coloured grey. (b) Front view of the square canyon with trees and planar view of the square canyon without (c) and with (d) trees. (e) Front view of the large canyon with trees and planar view of the large canyon without (f) and with (g) trees. The blue rectangles in panels (b) and (e) indicate the position of the measuring section in the transversal section of the canyon.

and z -axes are oriented in the streamwise, transversal, and vertical directions, respectively (see the red arrows in figure 1a).

Vegetation was simulated using miniature trees (the same ones used in Fellini et al. 2022 and Del Ponte et al. 2024) with a trunk height of 2 cm and a crown 6.5 cm high and 4.5 cm wide, as shown in figure 1b. At a 1:200 scale, these models represent trees that are 17 m tall and 9 m wide (e.g., plane trees,

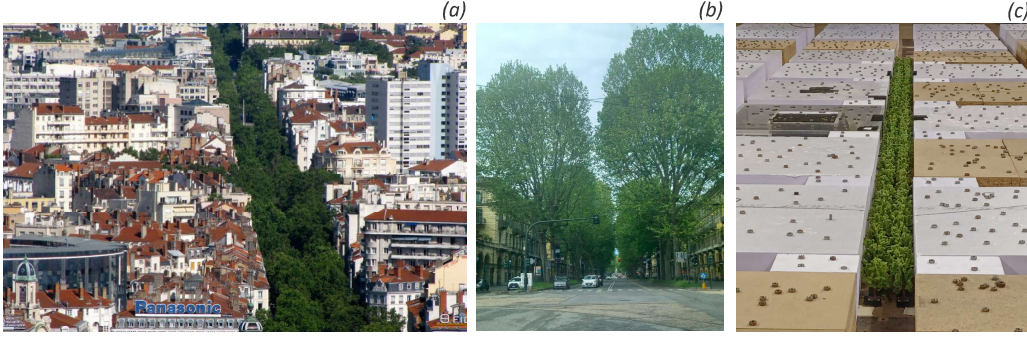


Fig. 2 (a) Tree-lined boulevard in Paris. Source: *Avenue lined with trees in Paris* by K.G.Hawes/Flickr. (b) Tree-lined boulevard in Turin. (c) Tree-lined street canyon modeled in the wind tunnel.

horse chestnuts), typical of those found along the boulevards of European cities. The aerodynamic properties of the model trees are characterized by an aerodynamic porosity of 0.3 and a drag coefficient of 1.1 (Fellini et al. 2022), values comparable to natural trees (Manickathan et al. 2018). Note that the miniatures do not have leaves distinct from the branches and this prevents us from evaluating a real leaf area density (e.g., we are not able to evaluate the momentum adsorption capacity *sensu* Kunadi et al. 2024). To achieve a homogeneous vegetation cover, we arranged the model trees along the entire length of the lateral walls of the reference canyon in three different configurations: no trees in the canyon (Zero configuration, figure 1c,f), two parallel rows of trees spaced 14 cm apart (Half configuration), and two parallel rows of trees spaced 7 cm apart (Full configuration, figure 1d,g), with spacing measured along the x -axis. We used the canyon with $H/W=1$ to simulate dense vegetation cover with intersecting crowns, typical of European cities (Fig. 2), and the canyon with $H/W=0.5$, to simulate large boulevards with sparser vegetation, easier to see in the majority of cities worldwide.

2.2 Measurement techniques

The boundary layer above the obstacles was characterized using a Hot-Wire Anemometer (HWA) equipped with a X-wire probe with an acceptance angle of $\pm 45^\circ$, allowing for the simultaneous measurement of two velocity components: the longitudinal velocity u , along the x -axis, and the transversal velocity v , along the y -axis. The platinum probe wire is 1 mm long and with a diameter of $5 \mu\text{m}$. The instrument was calibrated by comparison with a Pitot tube. In addition, we placed a type K thermocouple close to the probe wire, to constantly monitor the temperature. A 2-minutes acquisition time at a frequency of 5000 Hz was used at each measurement point to ensure good convergence of the velocity statistics and well-resolved power spectra throughout the boundary layer.

The flow velocity within the reference street canyon was measured using a Laser Doppler Anemometer (LDA) Argon class IV, suited to characterize the velocity field within recirculating flow regions. This instrument is equipped with a 5 W power laser, emitting two blue and two green beams with wavelengths $\lambda_{blue}=488$ nm and $\lambda_{green}=514.5$ nm, respectively. The beams have a diameter of 0.1 mm and the LDA focal length is 400 mm. The dual-beam configuration allowed us to measure simultaneously the intensity of u and v . To measure the vertical velocity w , the LDA was coupled with a mirror. This configuration was exploited to measure Reynolds stresses above the obstacles, since the LDA provides a measure of them more precise than HWA in turbulent boundary layers (Marro et al. 2020). The flow was seeded with the fluid SAFEX®-Inside-Nebelfluid Dräger Spezial W, emitting droplets with dimensions in the range 0.5-2 μm .

To achieve a good convergence of the statistics of the velocity signal, we maintained a data rate between 800 and 2000 Hz – notably, the data rate tends to decrease towards the canyon floor, due to lower seeding –, setting a sampling time sufficiently long to collect at least 150000 values for each measuring point. These data rate and sampling time guarantee that the convergence of the mean, standard deviation, skewness, and kurtosis of the velocity signals has oscillation smaller than 5%. During the acquisition, the power of the blue and the green beams was set at 800 mW.

3 Preliminary experimental assessment

3.1 The boundary layer above buildings

In this section, we characterise the boundary layer developing above the urban canopy, analysing flow velocity statistics measured above the blocks. This characterization serves to demonstrate the Reynolds independence of the turbulent flow, the spatial homogeneity of the boundary layer above the reference canyon and its similarity with typical urban boundary layers, and to provide the parameters required for numerical modeling.

The boundary layer is $\delta = 0.9$ m high and it has free-stream velocity $U_\infty = 5 \text{ ms}^{-1}$. The characteristic Reynolds number of the flow is $Re_\delta = \delta U_\infty / \nu \simeq 2.9 \cdot 10^5$ (where $\nu \sim 1.52 \cdot 10^{-5} \text{ m}^2\text{s}^{-1}$ is the kinematic viscosity of the air at 19 °C) and the Reynolds numbers based on the obstacle height are equal to $Re_\infty = H U_\infty / \nu \simeq 3.3 \cdot 10^4$ and $Re_H = H \bar{u}_H / \nu \simeq 2 \cdot 10^4$, being \bar{u}_H the mean streamwise velocity at $z = H$. In a square canyon perpendicular to the external flow, the Reynolds independence condition is reached for $Re_\infty > 13000$ according to Allegrini et al. (2013) and for $Re_H > 3400$ according to Marucci and Carpentieri (2019). Additionally, Lin et al. (2021) reported that the criterion $Re_H > 11000$, set by Snyder (1972), holds for canyons with $H/W < 2.4$. Based on these findings, the values of Re_∞ and Re_H in the present experiment are sufficiently high to ensure a Reynolds-independent

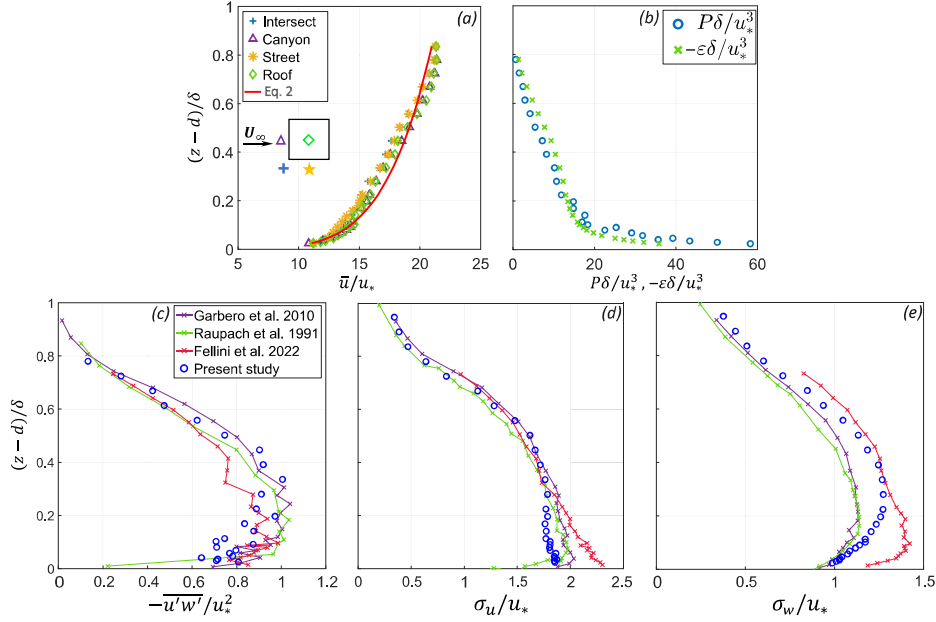


Fig. 3 (a) Vertical profiles of the mean longitudinal velocity, measured in four different positions around an obstacle (the white square represents an obstacle and the symbols around it indicate the positions). The red line represents the power law defined by Eq. 2. (b) Production and dissipation of t.k.e.. Comparison of the Reynolds stresses (c), longitudinal velocity standard deviation (d), and vertical velocity standard deviation (e), measured above the obstacles, with Raupach et al. (1991), Garbero et al. (2010), and Fellini et al. (2022). The vertical profiles from Garbero et al. (2010), Fellini et al. (2022), and from the present study are obtained as average over four different positions around an obstacle.

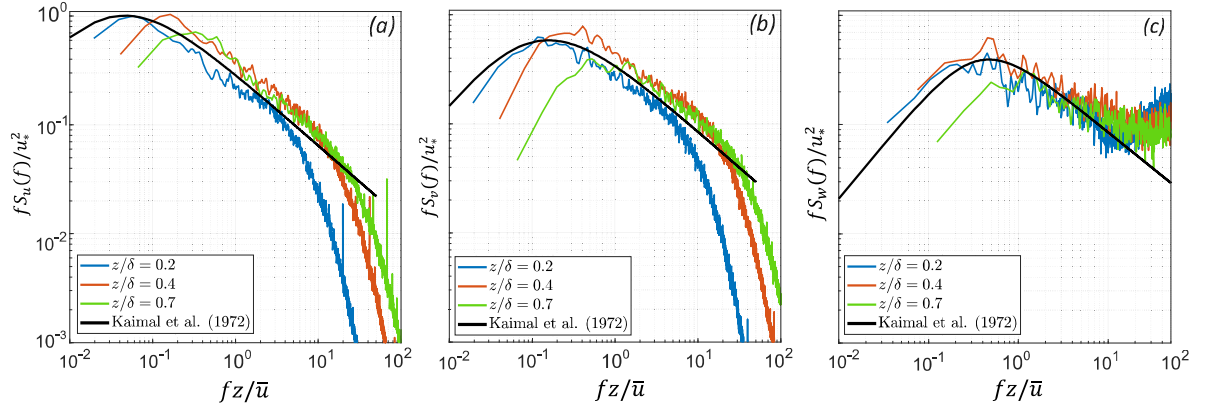


Fig. 4 Velocity spectra of the streamwise velocity (a), transversal velocity (b), and vertical velocity fluctuations (c), calculated above the obstacles, at different positions along the z -axis. The empirical spectra $S_u(f)$, $S_v(f)$, and $S_w(f)$ are compared with the model by Kaimal et al. (1972), extrapolated from field data and represented with a black line.

flow structure, especially considering that the characteristic velocity within a canyon aligned with the external flow is higher than in a perpendicular canyon.

We characterised the boundary layer flow measuring vertical profiles of flow velocity statistics above the obstacles, in different longitudinal and transversal positions in the wind tunnel. In Fig. 3a, we show vertical profiles of the mean streamwise velocity (\bar{u}) acquired in four different locations around an obstacle: on the rooftop (Roof), above a streamwise street (Street), above a spanwise street (Canyon), and above a street intersection (Intersect). These profiles were measured at a distance 10δ downstream the entrance of the test section, where the combined effect of the wake of the vortex generators and of the obstacle array placed at the ground has reached an equilibrium condition (Salizzoni et al. 2008). We can therefore consider that, above a so-called *blending height*, the velocity field can be considered as homogeneous in the horizontal plane. This is indeed confirmed by the overlapping between the profiles above the reference canyon, the perpendicular street, the intersection between the two and above a roof (see Fig. 3a). Note that we measured vertical profiles of flow velocity statistics adding different tree densities inside the streamwise street (reported in Fig. 4 in the Supplementary material) and we found that, outside the street, these profiles maintain the same shape of the ones measured above the empty canyon, demonstrating that the presence of trees has not significant effects on the turbulent flow above the obstacles. The mean longitudinal velocity at the top of the boundary layer $\bar{u}(x = \delta)$ measured at different longitudinal positions in the range $-1.6 < x/\delta < 2$ shows slight variations, with gradients in the range $0.01 < dU_\infty/dx < 0.04 \text{ s}^{-1}$.

More in detail, the lower part of the boundary layer is divided into two regions: the roughness sub-layer (below the blending height), where the flow is affected by the wakes of each single block, and the inertial sub-layer, where the flow statistics depend instead on the vertical coordinate, only. In the inertial region, the vertical profile of the mean streamwise velocity can be modeled by a logarithmic profile

$$\bar{u}(z) = \frac{u_*}{\kappa} \ln\left(\frac{z-d}{z_0}\right), \quad (1)$$

where u_* is the friction velocity, $\kappa \approx 0.4$ is the von Kármán constant, d is the zero-plane displacement length, and z_0 is the aerodynamic roughness length. We estimated u_* from the relation $u_*^2 = -\overline{u'w'}$ (Tritton 2012), where $\overline{u'w'}$ can be assumed equal to the average of Reynolds stresses in the range $2.25 \leq z/H \leq 4$, which is a plausible extent of the inertial layer (Oke et al. 2017), where the Reynolds stresses profile varies around a constant value. The parameters d and z_0 were estimated by least square fitting of Eq. 1 to the experimental data in the inertial layer with Eq. 1, with the value of u_* fixed (Salizzoni et al. 2008). We obtained $u_*/U_\infty = 0.047$ ($u_* = 0.25 \text{ ms}^{-1}$), $d/\delta = 0.11$ ($d = 0.098 \text{ m}$), and $z_0/\delta = 4.3 \cdot 10^{-4}$ ($z_0 = 3.9 \cdot 10^{-4} \text{ m}$). Note that the estimated values of d/H and z_0/H are in agreement with the empirical relation based on morphometrical parameters proposed by Grimmond and Oke (1999). The mean velocity throughout the whole boundary layer depth can be

instead modeled by a power law of the form (see red curve in Fig. 3a)

$$\bar{u}(z) = U_\infty \left(\frac{z-d}{\delta-d} \right)^n, \quad (2)$$

with an exponent $n = 0.18$ providing the best-fit to the experimental data.

In Fig. 3b, we present the profiles of turbulent kinetic energy (t.k.e.) production and dissipation. The t.k.e. dissipation was evaluated as $\varepsilon = \frac{15\nu}{\bar{u}} \left(\frac{\partial \bar{u}}{\partial z} \right)^2$, i.e. assuming local isotropy and adopting Taylor's hypothesis of frozen turbulence (Hinze 1967). The temporal derivative of $u'(t)$ was obtained from the velocity time series. The t.k.e. production was calculated as $P = -\overline{u'w'} \frac{\partial \bar{u}}{\partial z}$, using the vertical profiles of \bar{u} and $\overline{u'w'}$. The strong overlap between the two quantities indicates that, to a first approximation, the flow can be considered in local equilibrium, which is characteristic of boundary layer flows (Tennekes and Lumley 1972).

Panels 3c-3e show vertical profiles of Reynolds stresses, and longitudinal (σ_u) and vertical (σ_w) velocity standard deviation. These quantities, normalised by u_* , are compared to the reference profiles obtained by Raupach et al. (1991) and to the experimental profiles obtained by Garbero et al. (2010) and Fellini et al. (2022). The two latter reproduced an urban canopy similar to the present study, in the same wind tunnel. The $\overline{u'w'}$ and σ_u profiles agree well with the ones of the previous studies, even if there are discrepancies in the lowest part of the σ_u/u_* profiles (see panel 3d), due to the sensitivity to the roughness geometry and the experimental conditions (Raupach et al. 1991). Conversely, σ_w/u_* profiles (panel 3e) show significant difference from the other, depending on the geometry of the building array. As pointed out by Krogstad and Antonia (1999), this greater sensitivity of the vertical velocity fluctuations on the geometry of the wall is expected and has been previously observed for a variety of configurations of roughness elements.

Finally, in Fig. 4, we report the pre-multiplied spectra of the three components of velocity fluctuations – $u'(t)$, $v'(t)$, and $w'(t)$ –, calculated at increasing vertical distances from the obstacles. The power spectral density was evaluated applying the Welch method, to obtain well-resolved spectra. The velocity signals were re-sampled with a regular frequency of 5000 Hz and divided into 3000 windows, each filtered with the Hamming filter. The spectra, normalised by u_* and plotted against the non-dimensional frequency $n = fz/\bar{u}$ (where z is the position along the z -axis where the spectra were calculated and \bar{u} is the local mean longitudinal velocity), are compared to the empirical relations by Kaimal et al. (1972),

$$\frac{fS_u(f)}{u_*^2} = \frac{102n}{(1+33n)^{5/3}}, \quad \frac{fS_v(f)}{u_*^2} = \frac{17n}{(1+9.5n)^{5/3}}, \quad \frac{fS_w(f)}{u_*^2} = \frac{2.1n}{1+5.3n^{5/3}}, \quad (3)$$

obtained by fitting field measurements. We observe a strong overlap in both the production and inertial frequency ranges, indicating that the spectral energy

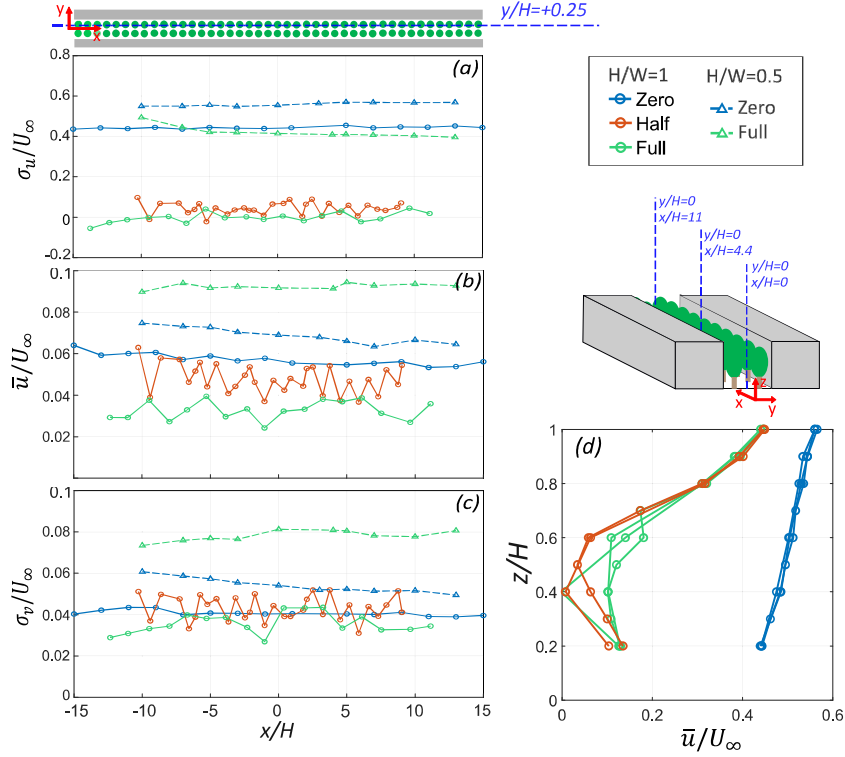


Fig. 5 Longitudinal profiles, measured in the square (continuous line) and large (dashed line) canyons at $y/H=+0.25$ and $z/H=0.4$, of the mean longitudinal velocity (a) and standard deviations of the longitudinal velocity (b) and transversal velocity (c). The Zero (blue), Half (orange), and Full (green) configurations are shown. The green circles in the sketch at the top of the figure indicate the position of the trees inside the canyon, spaced 7 cm apart. The position of the trees in the Half configuration can be deduced alternately removing half circles symmetrically with respect to the centre. The blue dashed line reported in the sketch indicates the transversal position with respect to the tree lines of the longitudinal profiles. (d) Vertical profiles of the mean longitudinal velocity, measured in the square canyon, at different longitudinal positions around $x/H=\{0,4.4,11\}$ (at $y/H=0$), in the Zero, Half, and Full configurations. The blue dashed line in the sketch provides an indicative representation of the positions of the vertical profiles.

317 distribution in the boundary layer developed during this experiment closely
 318 resembles that of a real atmospheric boundary layer.

319 3.2 Longitudinal homogeneity in the street canyon

320 As a first step, we verified that the velocity statistics within the canyon are
 321 invariant along the longitudinal direction, by measuring in the square canyon
 322 the velocity statistics along three longitudinal profiles $y/H=\{-0.25,0,0.25\}$, at

$z/H=0.4$. We measured also three vertical profiles of \bar{u} in the centre of the canyon (at $y/H = 0$), at different x -positions (at $x/H=\{0,4.4,11\}$). We repeated the analysis in the Zero, Half, and Full configurations. In Fig. 5, we report the longitudinal profiles of the mean longitudinal velocity and the standard deviation of the longitudinal and transversal (σ_v) velocity, at $y/H=0.25$, i. e. close to the left line of trees in the vegetated configurations (the profiles at $y/H=\{-0.25,0\}$ are available in the supplementary material). Both the mean and the standard deviation are normalized by the free-stream velocity (U_∞). In the empty canyon, \bar{u}/U_∞ , σ_u/U_∞ , and σ_v/U_∞ are homogeneous along the street axis (see blue profiles, in panels 5a-c). By adding trees (see orange and green profiles), the profiles become noisy, mostly with low tree density (orange profiles), even if the spatial pattern of the fluctuations can hardly be associated to the tree position. The t -test (Montgomery et al. 2021) shows that, regardless of the tree density, the \bar{u}/U_∞ , σ_u/U_∞ , and σ_v/U_∞ profiles do not exhibit (with significance level equal to 0.01) a linear trend along the x -axis of the canyon. The longitudinal homogeneity of the flow is also confirmed by the good overlap between the vertical profiles of \bar{u}/U_∞ measured at different x -positions (panel 5d).

Note that doubling the vegetation density (i. e., moving from the Half to the Full configuration) produces small longitudinal variations of \bar{u}/U_∞ (see the orange and green profiles in panels 5a and 5d) within the range $[0, 0.1]$. This variation is minimal compared to the substantial difference in mean velocity between a vegetated canyon (Half or Full configurations) and an empty canyon, where \bar{u}/U_∞ is around 0.4. Therefore, while increasing tree density from Half to Full leads to minor changes in the intensity and spatial behavior of the mean flow, the difference is small compared to the contrast observed between the empty and vegetated canyons. Turbulent intensities show more pronounced differences between the Half and Full configurations. In the Half configuration, σ_u/U_∞ values consistently fall between those of the Zero and Full profiles, while σ_v/U_∞ exhibits fluctuations similar to the Zero configuration. For these reasons, and for the sake of brevity, we will focus on the mean and turbulent flow fields in the Zero and Full configurations only. Four different configurations will be analysed: a square canyon (i) without vegetation (Fig. 1c) and (ii) with two parallel rows of trees with touching crowns (Fig. 1d), and a large canyon (iii) without trees (Fig. 1f) and (iv) with two rows of trees spaced 0.15 m apart (Fig. 1g).

We verified the longitudinal homogeneity of the velocity statistics also in the large canyon, measuring longitudinal profiles of \bar{u}/U_∞ , σ_u/U_∞ , and σ_v/U_∞ in the centre of the canyon ($y/H = 0$), in the Zero and Full configurations, only. In Fig. 5a-c (see the dashed lines) we can see that the profiles of both the mean longitudinal velocity and the turbulent velocity fluctuations show a small trend close to the entrance of the reference canyon (x/H in the range $[-10,0]$) due to the transition from aspect ratio $H/W = 1$ to $H/W = 0.5$. However, sufficiently far from the entrance of the canyon (i. e., $x/H > 0$), the longitudinal profiles of \bar{u}/U_∞ , σ_u/U_∞ , and σ_v/U_∞ do not show any statistically significant trend, as demonstrated by the t -student test with significance level 0.01.

Since the flow is statistically uniform along the x -axis, in the following we present the results of the velocity measurements on a single cross-section, located $20H$ from the canyon entrance (see blue dotted line in Fig. 1a). The horizontal resolution of the measuring grid was 2 cm, while the vertical resolution was 2 cm in the range $0.2 \leq z/H \leq 0.8$ and 1 cm in the range $0.8 \leq z/H \leq 1$, in order to capture the flow dynamics at the interface between the canyon flow and the external flow. To prevent laser beam reflections on the walls, measurements were conducted no closer than 1 cm from the vertical walls and 2 cm from the floor.

4 Turbulent flow field within the street canyon

To examine the influence of vegetation density and street geometry on street-canyon flow, we analyse the first four statistical moments of the velocity probability density function (pdf): specifically, the mean, standard deviation, skewness, and kurtosis of the longitudinal and transverse velocity time series, within the square (Sect. 4.1) and large (Sect. 4.2) canyons. For each geometry, we consider the empty (Zero) and the vegetated (Full) canyon configurations. Flow statistics are shown on the transversal section, by linearly interpolating the data. The mean and the standard deviation of the longitudinal and transversal velocity are normalized by the free-stream velocity U_∞ .

4.1 Square street canyon: $H/W=1$

In the empty canyon, the mean longitudinal velocity \bar{u} (panel 6a) shows a faster central core that decreases monotonically to zero towards the floor and the lateral walls. The mean transversal velocity \bar{v} (panel 6b) is zero in the whole section, highlighting a good alignment of the canyon with the external flow. The longitudinal velocity standard deviation σ_u (panel 6c) exhibits a crosswise increase, but the difference between the centre and the sides of the canyon is less marked than that observed for \bar{u} . In the vertical direction, σ_u/U_∞ decreases monotonically from around 0.08 at the rooftop, to 0.055 close to the ground. The vertical pattern of the transversal velocity standard deviation σ_v (panel 6d) is divided into two zones of almost homogeneous intensity: around 0.065 at the rooftop ($z/H=[0.9,1]$) and 0.04 within the canyon ($z/H=[0.2,0.8]$), showing a slight decreasing pattern towards the lateral walls. The gradient of σ_v/U_∞ at the rooftop denotes the presence of a shear layer, where local t.k.e. production leads to an increase of flow velocity fluctuations (Salizzoni et al. 2011; Fellini et al. 2020). The skewness of u and v (panels 6e and 6f, respectively) are almost zero on the whole cross-section, indicating symmetric fluctuations around the mean. The kurtosis of u (panel 6g) is quite homogeneous, showing values around to 3. A zero skewness and a kurtosis around 3 suggest a Gaussian-like behaviour of the pdf of the longitudinal velocity fluctuations. We assessed the similarity with a Gaussian distribution,

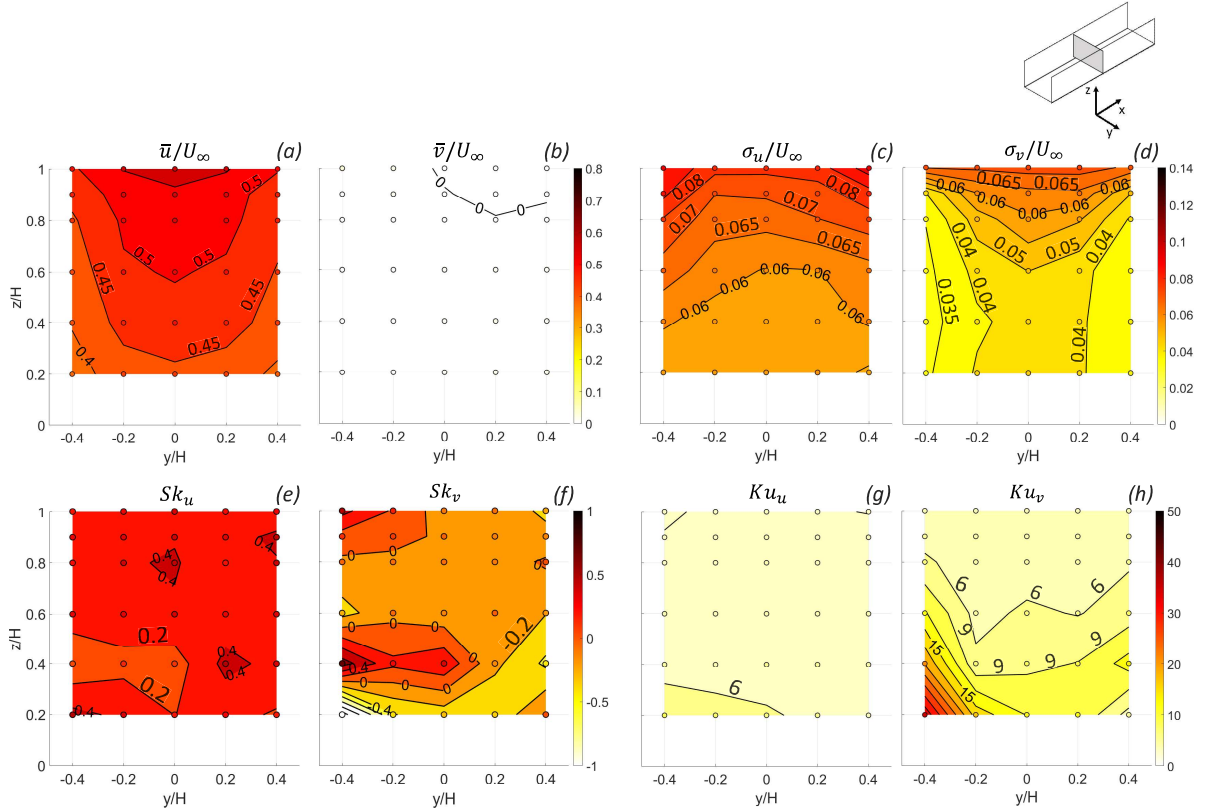


Fig. 6 Transversal behaviour, in the square canyon and in the Zero configuration, of the mean longitudinal velocity (a), mean transversal velocity (b), longitudinal velocity standard deviation (c), transversal velocity standard deviation (d), longitudinal velocity skewness (e), transversal velocity skewness (f), longitudinal velocity kurtosis (g), and transversal velocity kurtosis (h).

calculating the pdf of velocity time series acquired in the centre of the canyon and performing a Kolmogorov-Smirnov test with significance level 0.05. A deviation from the Gaussian arises in the lower left-hand corner of the cross-section, where Ku_u increases to 6. Conversely, the kurtosis of v (panel 6h) is not perfectly homogeneous across the measuring section, but it shows values around 9 along the transversal profiles at $z/H=\{0.2,0.4\}$, around 6 at $z/H=0.6$, and a peak around 30 in the lower left corner, suggesting fatter tails of the pdf of the transversal velocity fluctuations with respect to a Gaussian distribution. The slight asymmetries observed may be attributed to the sensitivity of the fourth-order statistical moment to minor inaccuracies in the arrangement of the building-like obstacles within the wind tunnel (Garbero et al. 2010; Fuka et al. 2018), as well as to the potentially imperfect alignment

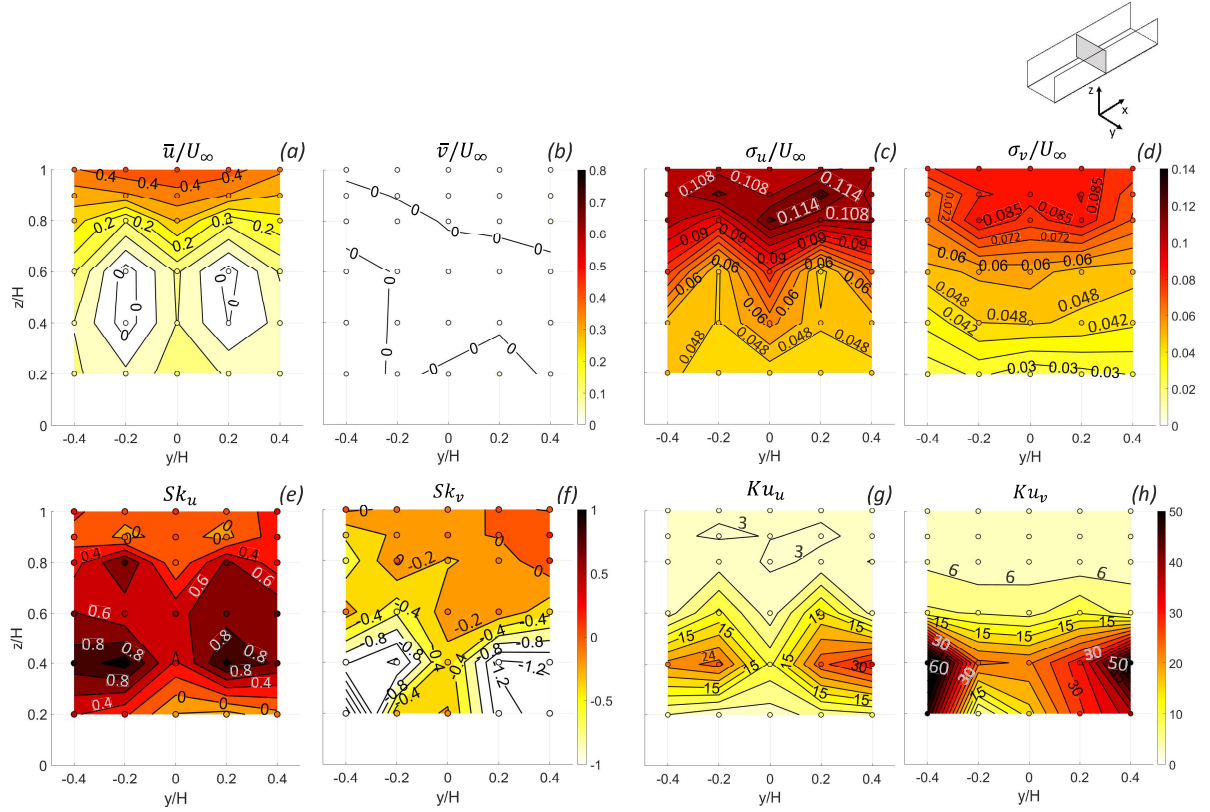


Fig. 7 Transversal behaviour, in the square canyon and in the Full configuration, of the mean longitudinal velocity (a), mean transversal velocity (b), longitudinal velocity standard deviation (c), transversal velocity standard deviation (d), longitudinal velocity skewness (e), transversal velocity skewness (f), longitudinal velocity kurtosis (g), and transversal velocity kurtosis (h).

of the external wind flow with the wind tunnel axis (Nironi et al. 2015; Carlo et al. 2024).

In the vegetated canyon, the flow channeling is significantly hindered. The spatial patterns of \bar{u}/U_∞ (Fig. 7a) exhibit two symmetric zones of nearly-zero values around the silhouettes of the trees (i.e., z/H in the range $[0.2, 0.8]$ and y/H in the ranges $[-0.4, 0]$ and $[0, +0.4]$ for the first and second tree, respectively) and a sharp increase in the mean velocity at the rooftop, where the external flow enters the canyon. Overall, the average mean longitudinal velocity in the cross-section $U_{t,exp} = 0.76 \text{ ms}^{-1}$ – calculated averaging the \bar{u} measurements resampled onto a 5 mm resolution grid using linear interpola-

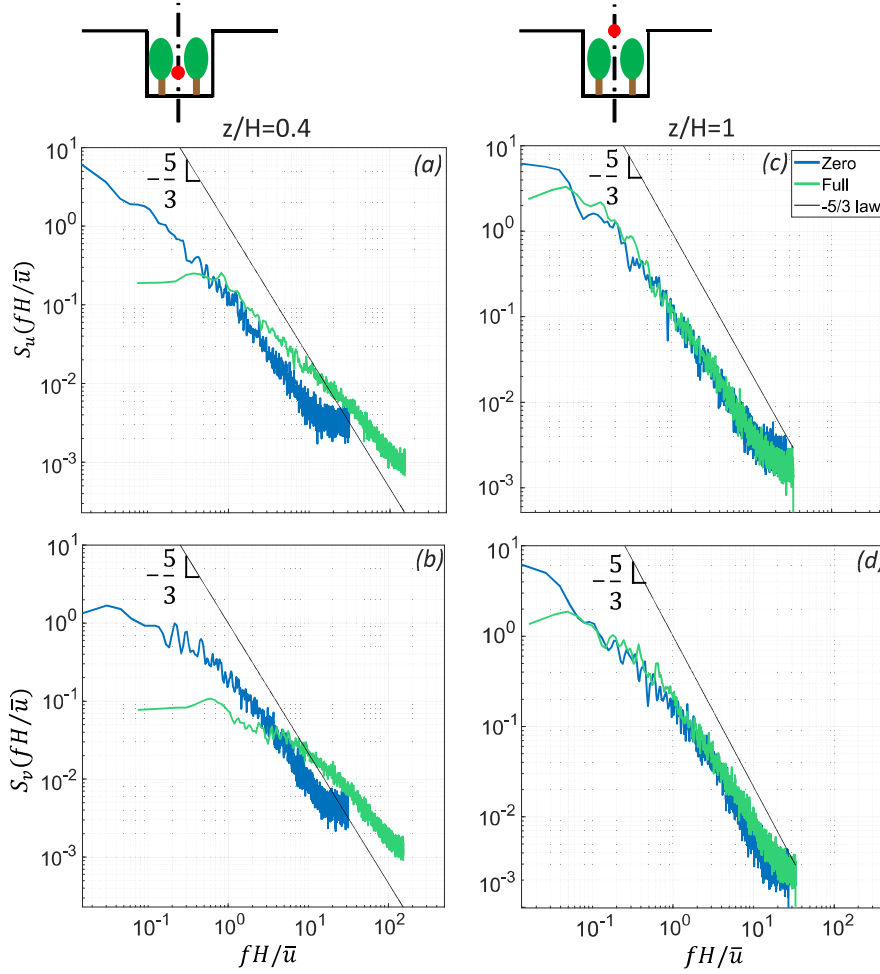


Fig. 8 Spectra of $(u(t) - \bar{u})/\sigma_u$ and $(v(t) - \bar{v})/\sigma_v$, measured along the vertical axis of the canyon ($y/H=0$), at $z/H=0.4$ (a,b) and $z/H=1$ (c,d), in the square canyon. The black line refers to the $-5/3$ law. The positions where the spectra were calculated are represented with the red dot in the sketches above the panels.

tion (subscripts ‘t’ and ‘exp’ recall the presence of trees and the experimental evaluation, respectively) – is 70% lower than the one in the non-vegetated canyon ($U_{exp} = 2.39 \text{ ms}^{-1}$). This substantial difference (found also by Maison et al. 2022) is primarily attributed to the obstruction caused by the trees. This is evident when quantifying the average mean longitudinal velocity in the region between the trees (evaluated considering \bar{u} measurements in the range $z/H=[0.2,0.6]$) which is 80% lower than the value calculated in the

empty canyon over the same area. At the rooftop level ($z/H=[0.8,1]$), however, this difference is reduced to 25%. The impact of the trees is also evident for σ_u (see Fig. 7c), which is amplified in the upper part of the tree crowns and above them, while being suppressed in the region surrounding the trees. Specifically, σ_u/U_∞ reaches intensities of approximately 0.11 in the upper part of the canyon — 30% higher than in the empty canyon — and around 0.05 around the tree silhouette, which is 15% lower than in the empty canyon at the same height range. In contrast, the pattern of σ_v/U_∞ (Fig. 7d) is relatively uniform across the canyon width but decreases steadily with height, ranging from 0.08 above the tree crowns, representing a 20% increase compared to the empty canyon, to approximately 0.03 near the ground. The increased turbulence at the canyon rooftop is driven by the interaction between the tree crowns and the external flow. Closer to the ground, the presence of trees dampens turbulent fluctuations and impedes the mean flow, as evidenced by the low values of both mean and turbulent velocities along the transverse profile at $z/H=0.2$, in panels 7a-d). This interaction can trap pollutants emitted at pedestrian level and reduce street ventilation. In contrast with the empty canyon, the third and fourth order moments (Fig. 7e and 7f) exhibit slight heterogeneity across the cross-section. Around the tree silhouette, the skewness of u (Sk_u) shows slightly positive values around 0.8, while the skewness of v (Sk_v) shows slightly negative values, around -1. ~~The slight heterogeneity of the skewness could be due to the formation of turbulent structures of heterogeneous sizes consequently to the vegetation-induced breaking up of large-scale eddies.~~ The correlation of this pattern with the vegetation silhouette suggests that skewness values different from zero could be induced by interaction between turbulent structures and vegetation elements. In the same region, the kurtosis of u (Ku_u) and v (Ku_v) reaches peaks up to 30 and 50, respectively (see panels 7g and 7h). Note that the spatial heterogeneity of Ku_u is more marked with respect to the one observed in the empty square canyon. However, the significant increase in kurtosis should be attributed to the reduction in velocity standard deviation between the trees, rather than to the presence of fatter tails in the velocity probability density function.

We can observe a quite similar spatial patterns of the mean and standard deviation of the longitudinal and transversal velocity within a canyon with half vegetation density (see the statistical moments measured in the Half configuration, reported in Fig. 3 of the supplementary material). Notably, we found a 80% decrease of \bar{u}/U_∞ with respect to the empty canyon in between trees, as well as an amplification of σ_u/U_∞ and σ_v/U_∞ at the canyon rooftop, due to the interaction between the tree crowns and the external flow. We estimated a 15% difference in the average mean longitudinal velocity in the cross-section between the Half and Full configurations (being $U_{t,exp}=0.90 \text{ ms}^{-1}$, in the Half configuration), which is negligible with respect to the difference between the Zero and Full configurations. The decrease in tree density leads to intensities of the skewness and kurtosis of u and v slightly higher in modulus with respect to the Full configuration. Notably, close to the ground Sk_u and Sk_v reaches maximum values around 5 and -6, respectively, and Ku_u and Ku_v around 60

and 80. Conversely, at the canyon rooftop (i.e., $z/H=[0.8,1]$), they recover values equal to zero and 3, respectively, as observed in the Full configuration. The difference in the intensity and spatial patterns of skewness and kurtosis, with respect to the Full configuration, arises probably due to the higher sensibility of these statistical moments to the displacement of the trees.

To investigate the turbulent scales involved in energy transport within both vegetated and non-vegetated canyons, we calculated the power spectral density of the longitudinal and transverse velocity time series. The Welch method was applied by resampling the velocity signals at a regular frequency of 1500 Hz and dividing them into 2500-point windows. In Fig. 8, we report the spectra of $u(t)$ and $v(t)$ calculated in two different positions along the vertical axis of the canyon ($y/H=0$): in between the tree crowns (at $z/H=0.4$, Fig. 8a,b) and above them (at $z/H=1$, Fig. 8c,d). In order to compare spectra among different positions and vegetation configurations, we forced all spectra to have the subtended area equal to 1, normalising the signals as $(u(t) - \bar{u})/\sigma_u$ and $(v(t) - \bar{v})/\sigma_v$. The spectra are plotted against the non-dimensional frequency fH/\bar{u} . Between tree crowns (panels 8a and 8b), the spectra in the vegetated canyon result shifted towards higher frequencies with respect to those calculated in the empty canyon. This suggests that the vegetation inhibits the formation of large-scale eddies. As a result, the energy transport is primarily driven by turbulent structures smaller than the transverse spacing between the tree rows W_{trees} , thus by length scales reflecting the canopy geometry (Poggi et al. 2004). The spectral content corresponding to W_{trees} can be read on the spectrum as the energy associated to the non-dimensional frequency $f'H/\bar{u} = 2.2$, where f' is the frequency corresponding to W_{trees} , calculated as $f' = \bar{u}/W_{trees}$. Moreover, in the presence of trees, the spectra do not exhibit a $-5/3$ Kolomogorov scaling in the inertial range. In the empty canyon, the spectra show an increase in energy associated with length scales larger than the canyon height (non-dimensional frequency smaller than 1), indicating that the turbulent flow is influenced by typical length scales of the inertial region of the external boundary layer (where the non-dimensional frequency associated with H is approximately $f_H z/\bar{u} \simeq 4$, being $f_H = \bar{u}/H$, as shown in the spectra S_u , S_v , and S_w of Fig. 4). Additionally, the spectra reveal the presence of superstructures that develop along the longitudinal direction of the canyon. Also without trees, the slope of spectra deviates from the $-5/3$ law, due to possible local production of tke at intermediate scales, induced by the generation of velocity gradients at the canyon boundaries. Above the tree crowns (panels 8c and 8d), both S_u and S_v cover the same range of frequencies and their slope is approximately $-5/3$, regardless of the presence of trees. The superposition between spectra suggests that the effect of trees on the energy transport is no more detectable at the canyon rooftop.

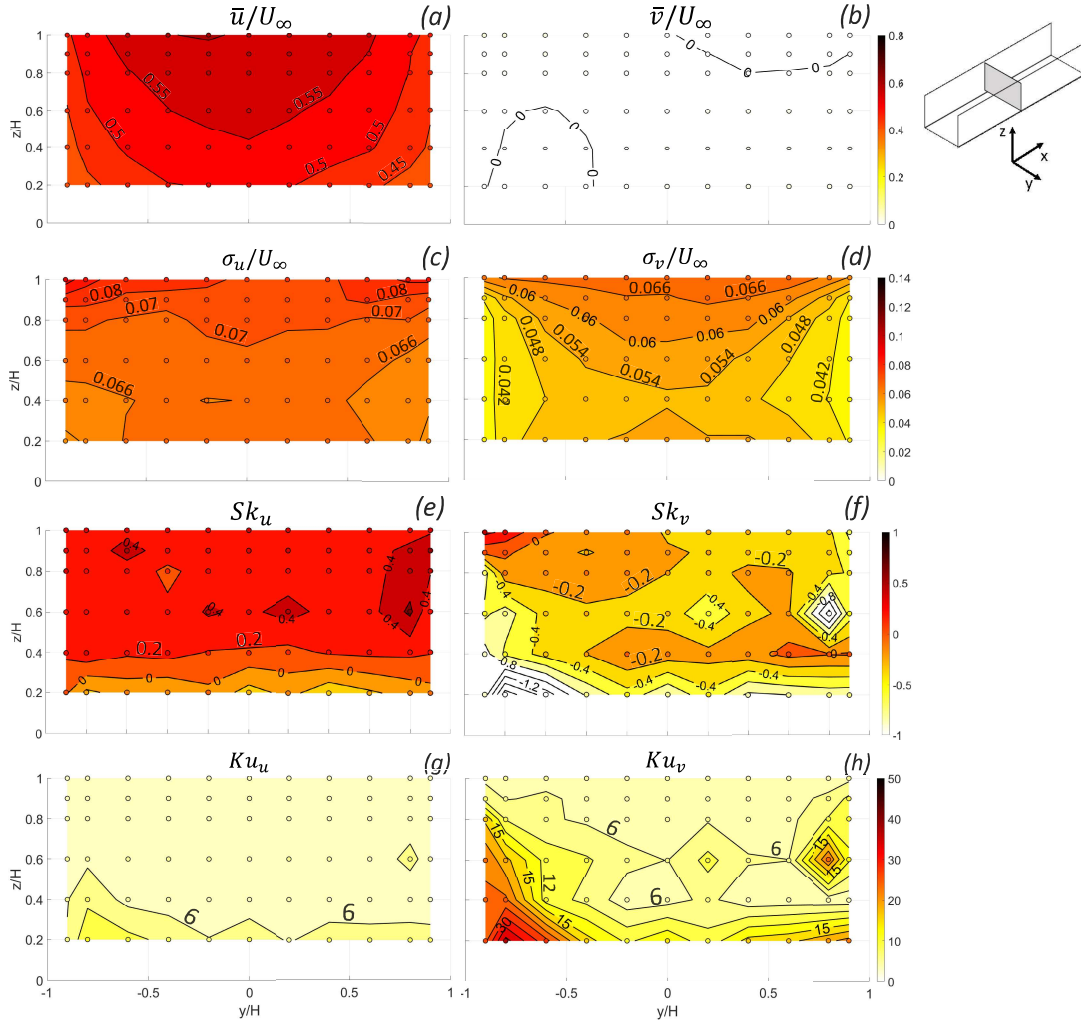


Fig. 9 Transversal behaviour, in the large canyon and in the Zero configuration, of the mean longitudinal velocity (a), mean transversal velocity (b), longitudinal velocity standard deviation (c), transversal velocity standard deviation (d), longitudinal velocity skewness (e), transversal velocity skewness (f), longitudinal velocity kurtosis (g), and transversal velocity kurtosis (h).

4.2 Large street canyon: $H/W=0.5$

In the large ($W = 2H$) canyon without trees, the mean longitudinal velocity (Fig. 9a) is relatively uniform up to approximately $0.15W$ from the lateral walls. Beyond this distance, the velocity decreases due to the influence of

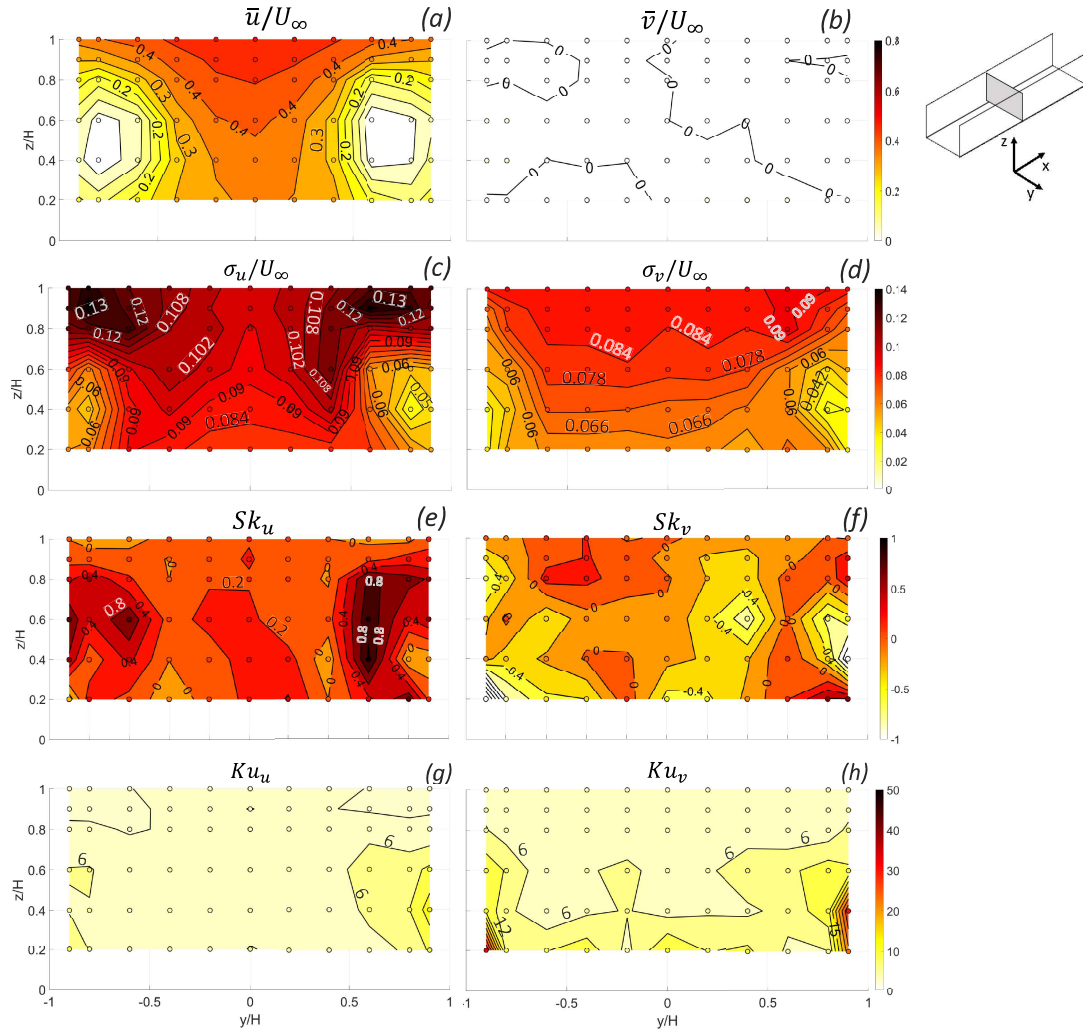


Fig. 10 Transversal behaviour, in the large canyon and in the Full configuration, of the mean longitudinal velocity (a), mean transversal velocity (b), longitudinal velocity standard deviation (c), transversal velocity standard deviation (d), longitudinal velocity skewness (e), transversal velocity skewness (f), longitudinal velocity kurtosis (g), and transversal velocity kurtosis (h).

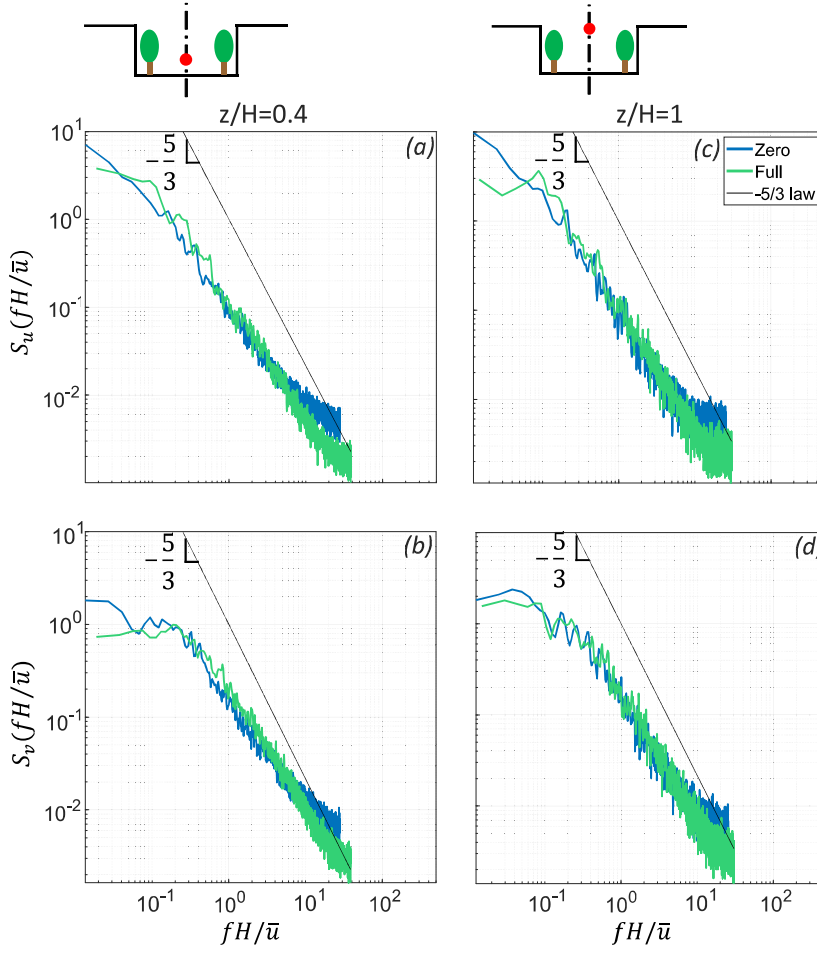


Fig. 11 Spectra of $(u(t) - \bar{u})/\sigma_u$ and $(v(t) - \bar{v})/\sigma_v$, measured along the vertical axis of the canyon ($y/H=0$), at $z/H=0.4$ (a,b) and $z/H=1$ (c,d), in the large canyon. The black line refers to the $-5/3$ law. The positions where the spectra were calculated are represented with the red dot in the sketches above the panels.

the walls. The transversal velocity \bar{v}/U_∞ (panel 9b) remains close to zero, indicating good alignment between the canyon and the external boundary layer. Values of σ_u/U_∞ (panel 9c) exhibit an almost symmetric spatial pattern, with intensities of 0.08 and 0.06 in the upper and lower corners, respectively, and around 0.07 in the center of the cross-section. The σ_v/U_∞ (panel 9d) shows a similar pattern to that observed in the square canyon (Fig. 6d), but with slightly higher values (around 0.05) at the centre of the canyon. The skewness values Sk_u and Sk_v are close to zero throughout the entire section (see panels

9e,f) and Ku_u (panel 9g) is homogeneous, with a value of 3, confirming the Gaussian distribution of u in the non-vegetated canyon, as observed in the square canyon. The skewness values Sk_u are close to zero throughout the entire section (see panel 9e), while Sk_v has slightly negative values around -1 in the lower left corner of the canyon (9f). The Ku_u (panel 9g) is 3 almost in the whole cross-section and 6 along the transversal profile at $z/H=0.2$, similarly to what found in the empty square canyon (Fig. 6g). The kurtosis of v (panel 9h) shows a heterogeneous pattern (similar to that observed in Fig. 6h). It is equal to 3 at the rooftop, while it peaks at approximately 30 in the lower left corner and around 15 in the lower right corner and along the lateral walls. The high values of Sk_v , Ku_u , and Ku_v are reasonably linked to the sensibility of high-order statistics to the change in aspect ratio at the entrance of the reference canyon, to be added to the sensibility to tiny errors in the experimental setup, as already mentioned for the square canyon.

In the tree-lined large canyon, the trees do not occupy the entire transverse section, creating a vegetation-free corridor in the central area. In this corridor, the mean longitudinal velocity (Fig. 10a) is 25% lower than in the empty large canyon, and 70% higher than in the areas between the trees in the square canyon. Conversely, around the trees, \bar{u}/U_∞ drops sharply to zero, as observed in the square canyon (see white areas in figure 7a). The spatial average of the mean longitudinal velocity in the vegetated large canyon $U_{t,exp} = 1.39 \text{ ms}^{-1}$ is nearly half that of the empty large canyon ($U_{exp} = 2.63 \text{ ms}^{-1}$). This difference is smaller than the one observed between the empty and vegetated square canyons. A considerable heterogeneous pattern also characterises the velocity standard deviation: both σ_u/U_∞ and σ_v/U_∞ are reduced around the trees but higher above the tree crowns and in the vegetation-free corridor compared to the empty large canyon. Above the tree crowns, σ_u/U_∞ (panel 10c) reaches 0.13, while in the centre of the canyon, it shows a monotonic vertical decrease from 0.1 at the rooftop to 0.08 at the ground. Examining the spatial pattern of σ_v/U_∞ , the influence of the trees is again evident, with values of 0.04 near the canyon walls and 0.09 and 0.06 in the upper and lower parts of the vegetation-free corridor, respectively. The increase in velocity turbulent fluctuations, observed in the vegetation-free corridor, is likely due to sparser vegetation cover in the transverse direction, which enhances the surface roughness and hence turbulence generation within the large canyon (Zhao et al. 2023b; Peltola et al. 2025), resulting in more efficient turbulent mixing compared to the square canyon. The presence of trees has not a unique enhancing effect on the third and fourth moments, as we observed in the square vegetated canyon, since the presence of trees attenuates some high values of skewness and kurtosis caused by imperfections in the canyon geometry and wind-canyon misalignment. The skewness of u (Fig. 10e) increases to 0.8 around the trees, as we observed in the square vegetated canyon, while it is not possible to identify a clear imprint of trees in the Sk_v pattern (Fig. 10f). The kurtosis of u (Fig. 10g) shows values equal to 3 across the most of the cross-section and it slightly increases to 6 around the right-hand tree and in a smaller area around the left-hand tree. The skewness and the kurtosis of u shows typical Gaussian

distribution values in the vegetation free-corridor. The Ku_v (Fig. 10h) exhibits a quite heterogeneous pattern: it is equal to 3 and 6 at the rooftop and in between the trees, respectively, and it reaches approximately 10 at $z/H=0.2$ and around 15 in the lower left and right corners. In contrast to what observed in the square vegetated canyon, the Ku_v in the lower left corner of the large vegetated canyon is lower than in the empty large canyon and these intensities are comparable in the lower right corner.

In Fig. 11, we present the power spectral density of $(u(t) - \bar{u})/\sigma_u$ and $(v(t) - \bar{v})/\sigma_v$ calculated in the centre of the canyon, at $z/H=0.4$ (panels 11a,b) and $z/H=1$ (panels 11c,d). For both S_u and S_v , the spectra from the empty and vegetated canyons show good overlap at both z/H levels, in contrast to the differences observed at $z/H = 0.4$ in the square canyon (see Fig. 8a,b). This suggests that the influence of trees on the energy spectral content in a large canyon is confined to the lateral walls, becoming weaker toward the centre of the canyon. Regardless of the presence of trees, the largest energy content of S_u and S_v is associated to length scales larger than H , as observed in the empty square canyon. As we observed in the square canyon, the spectra show a slope different from $-5/3$ at $z/H=0.4$, ~~due to a lack of separation between large and small turbulent scales within the canyon flow~~, and they get closer to the $-5/3$ Kolmogorov scaling at the rooftop.

5 Analytical modeling

The aim of this section is twofold. First (Sect. 5.1), we use data from the empty canyon to evaluate the predictions of the analytical model by Soulhac et al. (2008), which describes the spatial distribution of the mean velocity across the canyon section. This analytical model has been validated by comparison with results from numerical simulation performed with the Reynolds-Averaged Navier–Stokes model MERCURE. In the present study, we present the first comparison with experimental data. Next (Sect. 5.2), we apply data from the vegetated canyons to estimate the friction coefficients associated with the drag exerted by trees on the canyon flow. In this second analysis, we focus solely on the bulk flow velocity, averaged across the canyon section. The development of a more detailed model for the mean velocity’s dependence on the spatial coordinate within a vegetated canyon will be the subject of future work.

5.1 Empty canyon

The model by Soulhac et al. (2008) provides an analytical solution for the mean longitudinal velocity $\bar{u}(y, z)$ within an indefinitely long two-dimensional canyon parallel to the external flow, as a function of the canyon geometry and the roughness of the walls (z_i). The main assumptions of the model are: (i) the mean velocity field within a canyon, having height H and width W , is governed by turbulent entrainment at roof level of momentum from the

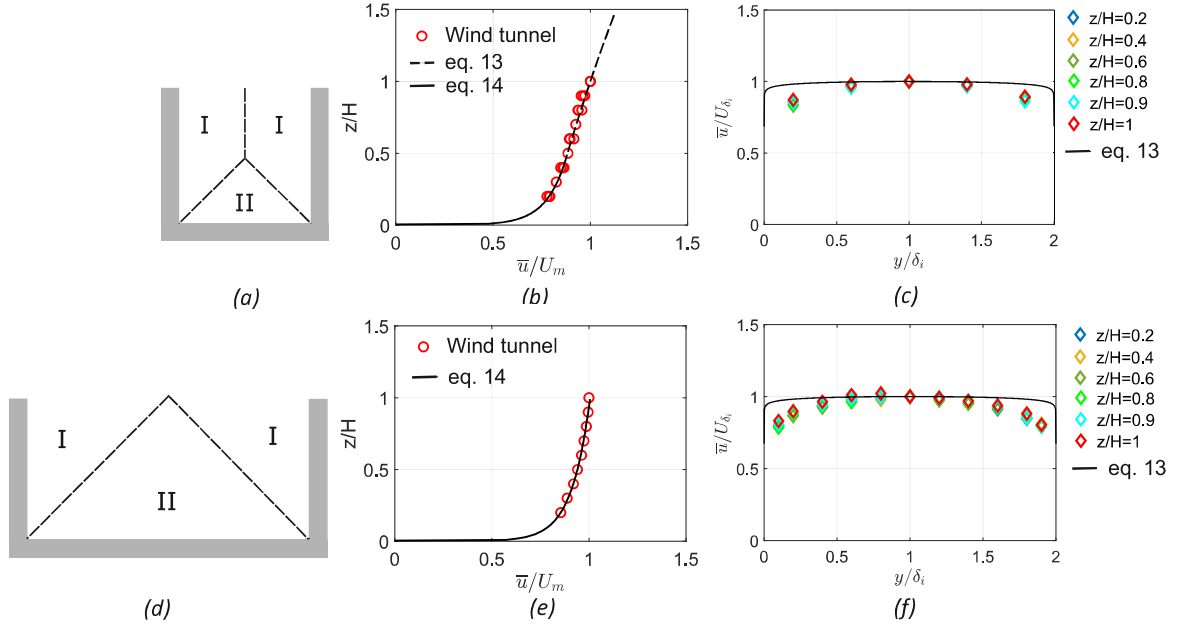


Fig. 12 (a) Sketch of the partition of the flow in the square canyon according to the analytical model. Comparison between the vertical profiles of \bar{u}/U_m acquired in the centre of the canyon ($y/H=0$), at the longitudinal positions $x/H=\{0,4.4,11\}$, with Eqs. 13-14 (b) and of the horizontal profiles of \bar{u}/U_{δ_i} with equation (13) (c). (d) Same sketch as (a) for the large canyon. Vertical (e) and horizontal (f) experimental profiles, measured in the large canyon, overlapped with Eqs. 14 and 13, respectively

external boundary layer, (ii) the longitudinal pressure gradient is negligible, i. e. $\partial P/\partial x = 0$, and (iii) no transverse components of the flow are considered. To model the spatial distribution of $\bar{u}(y, z)$, the flow within the canyon is divided into two regions (see Figs. 12a and 12d for the square and large canyons, respectively): Region I, where the flow is influenced by the side walls, and Region II, where the flow is influenced by the ground. The flow dynamics in Region I and II are assumed independent of each other and influenced by the nearest rigid boundary, only. The no-slip condition is imposed on the canyon walls and floor, thus the interaction between the mean flow and the canyon walls generates boundary layers, whose thickness δ_i depends on the canyon geometry, according to the relation $\delta_i = \min(H, W/2)$. Based on assumptions (i), (ii), and (iii), the longitudinal component of the Navier-Stokes equation writes

$$\frac{\partial \overline{u'v'}}{\partial y} + \frac{\partial \overline{u'w'}}{\partial z} = 0. \quad (4)$$

By solving Eq. 4 using the gradient-diffusion approach to model Reynolds stresses and applying the method of separation of variables, the time-averaged

longitudinal velocity in I (i.e., $z > \delta_i$) is given by:

$$\frac{\bar{u}(y, z)}{U_m} = f\left(\frac{y + W/2}{\delta_i}\right)g\left(\frac{z}{\delta_i}\right), \quad (5)$$

where U_m is the mean longitudinal velocity at the centreline of the rooftop (i.e., $y = \delta_i$ and $z = H$) and the g and f functions are the vertical and horizontal profiles of \bar{u}/U_m , respectively. In Region II ($z \leq \delta_i$), the mean longitudinal flow is modeled as a boundary layer over a rough wall. Details about the equations of the model are reported in Appendix 1.

The analytical model is here compared with the experimental vertical and horizontal profiles of \bar{u} , measured in the non-vegetated square and large canyons. We used three vertical profiles of \bar{u} , measured in the centre of the square canyon at different x -positions (i.e. the blue profiles in Fig. 5d), and one profile measured in the centre of the large canyon. The experimental vertical profiles of \bar{u} are normalised by $U_m = \bar{u}(y/H = 0, z/H = 1)$. The horizontal profiles are extracted from the cross-sections (Fig. 6a and 9a) and normalised by the mean longitudinal velocity at $y = \delta_i$ at each z level (denoted as U_{δ_i}). The comparison is made by fitting the experimental profiles to the analytical ones, with the unknown parameters C and z_i (see Appendix 1), treated as free parameters.

In the square canyon (Fig. 12b), we found a good agreement between the experimental vertical profiles of \bar{u}/U_m and the analytical model, with $C = 0.18$ and $z_i = 1.01 \cdot 10^{-5}$ m. Conversely, when maintaining the same C and z_i , the experimental horizontal profiles of \bar{u}/U_{δ_i} do not overlap with the model close to the canyon boundaries (Fig. 12c).

A possible explanation for these discrepancies is twofold: first, the canyon walls lack significant aerodynamic roughness, and second, the presence of slight pressure gradients. Both factors challenge the foundational assumptions of the model, as they prevent the application of the method of separation of variables used to solve the Navier-Stokes equation (Eq. 4). This method, which establishes a relationship between the f and g functions through the constant C , may not hold under the experimental conditions of this study. The smooth nature of the canyon walls is evident from the small value of the roughness length ($z_i = 1.01 \cdot 10^{-5}$ m), which provides the best fit to the experimental data. The Reynolds number based on the wall roughness $Re_r = u_*^s z_i / \nu \simeq 0.1$ (being u_*^s the friction velocity at ground level, modeled with Eq. 15) is indeed lower than the typical Re_r of a fully rough turbulent flow (Snyder and Castro 2002). To investigate the presence of potential pressure gradients, we calculated the two terms of the divergence of the stress tensor $\partial \bar{u}'v'/\partial y$ and $-\partial \bar{u}'w'/\partial z$ (see Eq. 4) along a single vertical profile in the centre of the canyon. Our analysis revealed slight discrepancies between the two profiles, indicating the presence of a modest pressure gradient in the range $-0.6 < dP/dx < -0.05$ Pa m⁻¹ along the wind tunnel. These findings align with the subtle variations in U_∞ observed along the wind tunnel axis (see Sect. 3.1).

By integrating the model across the entire cross-section of the canyon, Soulhac et al. (2008) derive an analytical equation for the average mean lon-

gitudinal velocity in the cross-section of the canyon U_{street} (see Appendix 1). Given the canyon geometry, along with the previously obtained values of U_m , C , and z_i , the analytical solution provides $U_{street} = 2.32 \text{ ms}^{-1}$ for the square canyon. This value is in close agreement with the experimental $U_{exp} = 2.39 \text{ ms}^{-1}$ (reported in Sect. 4.1), which is obtained by integrating the available point measurements across the cross-section, excluding data near the canyon walls that could not be measured due to instrument constraints. To improve the accuracy of U_{exp} , an attempt was made to extrapolate the missing data near the canyon boundaries using a logarithmic law, applying the no-slip condition at the walls. After this operation, the experimental U_{exp} becomes 1.96 ms^{-1} , which is 15% lower than the analytical U_{street} . This result indicates that the model provides a reliable estimate of the average mean longitudinal velocity in the cross-section of the canyon. The discrepancy between U_{exp} and U_{street} can be attributed to differences between the analytical and experimental horizontal profiles of \bar{u}/U_m near the canyon walls, as well as uncertainties in the extrapolation of the missing experimental data.

With the same procedure, we tested the model in the large canyon. Figure 12e shows a good overlap between the experimental \bar{u}/U_m profile and the analytical model with $z_i = 2.4 \cdot 10^{-5} \text{ m}$, which is slightly larger than the value estimated for the square canyon. The excellent match between the experimental and analytical vertical profiles supports further the assumption that the flow within the canyon can be divided into two regions: Region I, influenced by the side walls, and Region II, influenced by the floor. Furthermore, it confirms that the thickness of the internal boundary layers depends on the canyon's aspect ratio. However, when examining the horizontal profiles of \bar{u}/U_{δ_i} (Fig. 12f), we observe that the experimental data do not align with the analytical model near the lateral walls (the possible reasons are the same as those indicated above for the square canyon).

The analytical U_{street} in the large canyon is 2.42 ms^{-1} , which is only 5% higher than the experimental $U_{exp} = 2.30 \text{ ms}^{-1}$, calculated after having extrapolated the missing data near the canyon walls using a logarithmic law. The agreement between the experimental and analytical spatially-averaged mean longitudinal velocity is better in the large canyon compared to the square canyon. This is likely because, as the H/W ratio decreases, the discrepancy between the model and experimental mean velocity near the lateral walls becomes less significant in influencing the overall mean velocity across the entire cross section.

5.2 Vegetated canyon

To quantify the global impact of trees on airflow, we assess the bulk momentum balance—considering averaged quantities across the canyon section—per unit length along the canyon axis. This evaluation follows the methodology outlined by Soulhac et al. (2008). Specifically, under the assumptions (i), (ii), and (iii)

Table 1 Estimated pressure loss coefficients from different literature studies. The values are reported at full scale

References	λ_t [m ⁻¹] $H/W=1$	λ_t [m ⁻¹] $H/W=0.5$
This study	0.014	0.004
Majumdar et al. (2024)	0.0085	0.0025
Gromke and Ruck (2012) ^a	[0.53,1.33]	[0.53,1.33]
Jeanjean et al. (2015) ^b	[0.11,0.65]	[0.11,0.65]

^a This study provides values of λ_t varying the vegetation porosity.

^b This study provides values of λ_t varying the Leaf Area Density.

723 detailed in Sect. 5.1, the momentum budget is expressed as:

$$W\tau_H - \frac{1}{2}HW\rho\lambda_w U_{t,exp}^2 - \frac{1}{2}HW\rho\lambda_t U_{t,exp}^2 = 0 \quad (6)$$

724 where $\tau_H = u_*^2 \rho$ is the shear stress exerted by the external flow at $z = H$, ρ is
 725 the air density, λ_w is the pressure loss coefficient of the building walls, λ_t is the
 726 pressure loss coefficient of the trees (Buccolieri et al. 2009; Gromke and Ruck
 727 2012; Zhao et al. 2023a), and $U_{t,exp}$ is the average mean longitudinal velocity in
 728 the cross-section of the vegetated canyon, calculated averaging measurements
 729 linearly interpolated on a 5 mm resolution grid, to which zero velocity values
 730 were added at the canyon wall. The parameter λ_w , in Eq. 6, can be estimated
 731 from the momentum balance equation for the empty canyon (thus setting
 732 $\lambda_t = 0$ m⁻¹ and U_{exp} equal to 1.96 ms⁻¹ and 2.30 ms⁻¹ in the square and large
 733 canyons, respectively):

$$\lambda_w = \frac{2u_*^2}{HU_{exp}^2} \quad (7)$$

734 providing λ_w equal to 0.32 m⁻¹ for the square canyon and 0.24 m⁻¹ for the large
 735 canyon. The parameter λ_t characterising our model trees cannot be retrieved
 736 from the experiments, thus we estimate it as a function of $U_{t,exp}$, u_* , and
 737 H . Rearranging terms in the momentum balance (6), we obtain the following
 738 expression for the parameter λ_t :

$$\lambda_t = \frac{2u_*^2 - HU_{t,exp}^2\lambda_w}{U_{t,exp}^2 H} \quad (8)$$

739 where $u_* = 0.25$ ms⁻¹ and $U_{t,exp}$ is equal to 0.64 ms⁻¹ and 1.12 ms⁻¹, for the
 740 square and large canyons, respectively. Substituting these values, we obtain
 741 $\lambda_t = 2.73$ m⁻¹ in the square canyon and $\lambda_t = 0.76$ m⁻¹ in the large canyon.
 742 We observe that λ_t decreases with decreasing fraction of the cross-section of
 743 the canyon occupied by trees. In Table 1, we compare our estimates of λ_t with
 744 those reported in other studies. To do this, we need to convert our results
 745 at full-scale (Gromke and Ruck 2012; Zhao et al. 2023a). Since the scale of
 746 the experiment is 1:200, we obtain $\lambda_t = 0.014$ m⁻¹ in the square canyon and
 747 $\lambda_t = 0.004$ m⁻¹ in the large canyon.

The experimental estimate of λ_t can be compared to those from the analytical model by Majumdar et al. (2024), which estimates the drag exerted by trees on a turbulent flow. The model accounts for the horizontal momentum balance within a homogeneous vegetation canopy, considering velocity and pressure gradients, as well as the drag from the vegetation. According to Majumdar et al. (2024), in a longitudinally homogeneous flow, λ_t can be expressed as

$$\lambda_t = \frac{2c}{l_d}, \quad (9)$$

where l_d is the length of the tree drag, $c = \langle \bar{u}^2 \rangle_{yz} / U_{t,exp}^2$ and $\langle \bar{u}^2 \rangle_{yz}$ indicates the spatial average over the cross-section of the vegetated canyon of the mean longitudinal velocity squared. Assuming a same form for the advective term and longitudinal pressure gradient, the parameter l_d can be directly expressed as a function of the aerodynamic porosity:

$$l_d \left[1.27 + 0.55 \left(\frac{WH}{l_d^2} \right)^{0.33} \right] = - \frac{2L_T}{\ln(\alpha_t^2)} \quad (10)$$

where L_T is the length of the tree canopy and α_t is the aerodynamic porosity. To compare our estimates to those provided by Eq. 9, we assume that the cross-sections of the vegetated square and large canyons are similar to a homogeneous vegetation canopy of unit length, characterized by an homogeneous aerodynamic porosity. Since the aerodynamic porosity could not be estimated directly, we calculated the optical porosity ($\alpha_{op,c}$) of the vegetated cross-section and we exploited the empirical relation $\alpha_t = \alpha_{op,c}^{0.4}$, obtained by Guan et al. (2003) for infinitely long three-dimensional windbreaks. The optical porosity of the vegetated cross-section was then estimated as

$$\alpha_{op,c} = \frac{HW - [2(1 - \alpha_{op,t})H_T W_T]}{HW} \quad (11)$$

where H_T is the height of the model tree crown, W_T is the crown width, and $\alpha_{op,t} = 0.05$ is the optical porosity of the single model tree used in this study (Fellini et al. 2022). We obtained $\alpha_t = 0.72$ and $\alpha_t = 0.88$, for the square and large canyon, respectively. According to Eq. 10, we obtain $l_d = 2.29$ m and $l_d = 5.82$ m in the square and large canyons, respectively, and with Eq. 9 we evaluated $\lambda_t = 1.7$ m⁻¹ and $\lambda_t = 0.5$ m⁻¹ (with $c = 1.93$ in square canyon and $c = 1.48$ in the large canyon). These values (reported at full-scale in Table 1) are very similar to our experimental estimates, despite the trees being placed within an urban canyon. The discrepancies between the two estimates are likely to be due to uncertainties in the aerodynamic porosity estimate, as well as the fact that we neglected possible pressure and velocity gradients along the street canyon.

Other useful comparisons can be made with the results from Gromke and Ruck (2012) and Jeanjean et al. (2015). Gromke and Ruck (2012) modeled the aerodynamic effects of trees in wind-tunnel experiments using a porous foam material, assessing the material's aerodynamic characteristics through

the pressure loss coefficient. They found a pressure loss coefficient at full-scale equal to 0.53 m^{-1} for a pore volume fraction of 97.5% and equal to 1.33 m^{-1} for a pore volume fraction of 96%. Jeanjean et al. (2015) conducted CFD simulations to assess the effect of trees on pollution dispersion in the city of Leicester. They expressed the pressure loss coefficient at full scale as the product of the drag coefficient and the Leaf Area Density of real trees, obtaining a value of 0.4 m^{-1} . The values of λ_t found in this study are significantly smaller than those reported by Gromke and Ruck (2012) and Jeanjean et al. (2015). This can be explained by two features: i) Gromke and Ruck (2012) and Jeanjean et al. (2015) neglected the impact of canyon geometry, and ii) the model trees they used were made from foam material, with a porosity significantly lower than that of the three-dimensional model trees we adopted.

6 Conclusions

This study presents the results of a wind-tunnel study designed to quantify the aerodynamic effects of trees on the turbulent flow field within a street canyon, aligned with the external wind. Flow velocity measurements were conducted in both an empty canyon and a canyon with two rows of trees along the lateral walls. Additionally, we investigated the influence of the canyon aspect ratio, considering both a square canyon $H/W = 1$ and a large canyon $H/W = 0.5$.

In the vegetated square canyon, the mean longitudinal velocity decreases by 80% around the tree crowns and by 25% above them, compared to the empty canyon. Consequently, the average mean longitudinal velocity in the cross-section U_{exp} drops by 70% from the empty to the vegetated canyon. In contrast, in the upper part of the canyon, the interaction between the trees and the external flow leads to a 30% increase in longitudinal velocity fluctuations and a 20% increase in transversal velocity fluctuations, while both are dampened around the trees. Additionally, the presence of trees causes local kurtosis values significantly greater than 3, particularly in the lower corners of the canyon. As the aspect ratio of the canyon decreases, a vegetation-free corridor forms between the tree rows, where the mean longitudinal velocity and turbulent velocity fluctuations are 70% and 40% higher than in the center of the vegetated square canyon, respectively. Additionally, the difference in U_{exp} between the vegetated and non-vegetated large canyons is reduced to 50%. The spectra of the longitudinal and transversal velocity signals, calculated in the square canyon, show that, within the tree rows, energy transport is dominated by turbulent structures smaller than the transversal spacing between the tree lines. Furthermore, the spectra in this region do not resemble Kolmogorov spectra. In contrast, in the centre of the large canyon, the effect of the trees on the energy spectral content is less pronounced, and the energy associated with different length scales is similar, regardless of the presence of trees.

The data measured in the empty canyons $H/W = \{0.5, 1\}$ were compared with the analytical model developed by Soulhac et al. (2008). A good agreement was found between the experimental vertical profiles of the mean lon-

gitudinal velocity and the model equations. However, despite using the same fitting parameters, the horizontal profiles of \bar{u} did not match the analytical model near the canyon boundaries. Nevertheless, the difference between the experimental and analytical average mean longitudinal velocity in the cross-section was around 15% for the square canyon and 5% for the large canyon. Finally, we derived an expression for the pressure loss coefficient due to trees, which depends on the average mean longitudinal velocity in the cross-section of the vegetated canyon, the canyon height, and the friction coefficient of building walls. The coefficient λ_t was found to be 2.73 m^{-1} in the square canyon and to 0.76 m^{-1} in the large canyon. These values were derived by considering a momentum balance to the flow in the street canyon with miniatures of trees, evaluating experimentally the average mean longitudinal velocity along the canyon. The obtained λ_t deviates from other literature studies due to the absence of the canyon walls in their models, different types of vegetation, and possible longitudinal pressure or velocity gradients, neglected in the momentum balance.

We reported the first comparison of the analytical model by Soulhac et al. (2008) with experimental data. The positive outcomes of the comparison regarding the spatial average mean longitudinal velocity along the canyon (i.e., U_{street}) are an important results of this work. In fact, they reinforce the validity of using this analytical relation in the operational urban dispersion model SIRANE, to parameterize the advective flux along the street axis (Soulhac and Salizzoni 2010; Soulhac et al. 2011). Furthermore, the SIRANE model does not account for the presence of obstacles within the streets (i.e., trees), thus our estimate of the pressure loss coefficient by means of experimental data may be a step forward to parametrize the mean advective flux along a vegetated streets.

From the analysis of the turbulent flow field, we can conclude that high-density tree boulevards, where the crowns are in close contact crosswise, significantly impede both the mean and turbulent flow within the canyon. This challenges the idea that a wind direction perpendicular to the canyon axis is the worst-case scenario for air quality in urban canyons. By reducing the H/W ratio, a sparser vegetation cover increases the surface roughness, leading to higher turbulent fluctuations and more efficient turbulent mixing in the centre of the larger canyon compared to the narrower one. These findings can be included in urban design strategies, to ameliorate the ventilation of urban street canyons. However, it is not possible to assess the effect of trees and canyon geometry on the efficiency of vertical momentum transport between the canyon and the external flow, as this study does not provide a characterization of the vertical velocity field. This limitation arises from the difficulty of introducing the Laser Doppler Anemometry (LDA) system coupled with a mirror (necessary for measuring the vertical velocity component, w) into the vegetated canyon.

In addition to vegetation density, several other factors influence ventilation within urban canyons, including street geometry, the presence of street intersections, and wind direction. To explore these mechanisms further, we are cur-

rently analysing flow velocity measurements collected within canyons inclined at 30° and 60° with respect to the external wind, as well as canyons with street intersections. Furthermore, another experimental campaign is planned to investigate the combined effects of trees, street geometry, and wind direction on the vertical ventilation velocity within the street canyon.

Acknowledgements The authors would like to express their gratitude to Horacio Correia for his invaluable assistance in the execution of the wind tunnel experiments. PS would like to acknowledge the Auvergne-Rhône-Alpes Region for funding the VEB-MU project. SF and PS would like to acknowledge the Università Italo-Francese for their financial support of the BreathEasier project (Galileo 2024 call).

Appendix 1: Details on the Soulhac et al. (2008) model

In Region I (see panels 12a and 12d), the time averaged longitudinal velocity is written as

$$\frac{\bar{u}(y, z)}{U_m} = f\left(\frac{y + W/2}{\delta_i}\right)g\left(\frac{z}{\delta_i}\right) \quad (12)$$

where U_m is the mean longitudinal velocity at the centreline of the rooftop (i.e., $y = \delta_i$ and $z = H$), δ_i is the thickness of the boundary layers developed on the canyon walls, and the functions f and g read

$$\begin{cases} f\left(\frac{y+W/2}{\delta_i}\right) = \frac{J_1(C)Y_0\left(\frac{C(y+W/2)}{\delta_i}\right) - J_0\left(\frac{C(y+W/2)}{\delta_i}\right)Y_1(C)}{J_1(C)Y_0(C) - J_0(C)Y_1(C)} \\ g\left(\frac{z}{\delta_i}\right) = \exp\left[\frac{C}{\sqrt{2}}\left(\frac{z}{\delta_i} - \frac{H}{\delta_i}\right)\right] \end{cases} \quad (13)$$

where J_0 , Y_0 , J_1 , and Y_1 are Bessel functions, C is a constant, H is the canyon height, and W is the canyon width. In Region II, the mean longitudinal flow is modeled as a boundary layer over a rough wall

$$\frac{\bar{u}(z)}{U_m} = \frac{u_*^s}{\kappa} \ln\left(\frac{z}{z_i}\right) \quad (14)$$

where $\kappa=0.4$ is the von Kármán constant, z_i is the wall roughness, and u_*^s is the friction velocity at ground level, obtained forcing the profile of Region II matching the one of Region I, at the interface between the two regions

$$u_*^s = \frac{\kappa}{\ln\left(\frac{\delta_i}{z_i}\right)} \exp\left[\frac{C}{\sqrt{2}}\left(1 - \frac{H}{\delta_i}\right)\right]. \quad (15)$$

By using Eq. 12-15, the average mean longitudinal velocity in the cross-section of the canyon

$$U_{street} = \frac{1}{HW} \int_0^H \int_{-W/2}^{W/2} \bar{u}(y, z) dy dz, \quad (16)$$

reads (Soulhac et al. 2008)

$$U_{street} = U_m \frac{\delta_i^2}{HW} \left[\frac{2\sqrt{2}}{C} (1-\beta) \left(1 - \frac{C^2}{3} - \frac{C^4}{45} \right) + \frac{\beta(2\alpha-3)}{\alpha} + \left(\frac{W}{\delta_i} - 2 \right) \left(\frac{\alpha-1}{\alpha} \right) \right] \quad (17)$$

where α and β are equal to

$$\begin{cases} \alpha = \ln\left(\frac{\delta_i}{z_i}\right) \\ \beta = \exp\left[\frac{C}{\sqrt{2}}\left(1 - \frac{H}{\delta_i}\right)\right]. \end{cases} \quad (18)$$

References

- Aboelata A, Sodoudi S (2020) Evaluating the effect of trees on UHI mitigation and reduction of energy usage in different built up areas in Cairo. *Building and Environment* 168:106–490
- Allegrini J, Dorer V, Carmeliet J (2013) Wind tunnel measurements of buoyant flows in street canyons. *Building and Environment* 59:315–326
- Beckett KP, Freer-Smith P, Taylor G (2000) Particulate pollution capture by urban trees: Effect of species and windspeed. *Global change biology* 6(8):995–1003
- Buccolieri R, Gromke C, Di Sabatino S, Ruck B (2009) Aerodynamic effects of trees on pollutant concentration in street canyons. *Science of the Total Environment* 407(19):5247–5256
- Buccolieri R, Salim SM, Leo LS, Di Sabatino S, Chan A, Ielpo P, de Gennaro G, Gromke C (2011) Analysis of local scale tree–atmosphere interaction on pollutant concentration in idealized street canyons and application to a real urban junction. *Atmospheric Environment* 45(9):1702–1713
- Carlo OS, Fellini S, Palusci O, Marro M, Salizzoni P, Buccolieri R (2024) Influence of obstacles on urban canyon ventilation and air pollutant concentration: An experimental assessment. *Building and Environment* 250:111–143
- Del Ponte AV, Fellini S, Marro M, van Reeuwijk M, Ridolfi L, Salizzoni P (2024) Influence of street trees on turbulent fluctuations and transport processes in an urban canyon: a wind tunnel study. *Boundary-Layer Meteorology* 190(2):6
- Fellini S, Ridolfi L, Salizzoni P (2020) Street canyon ventilation: Combined effect of cross-section geometry and wall heating. *Quarterly Journal of the Royal Meteorological Society* 146(730):2347–2367
- Fellini S, Salizzoni P, Ridolfi L (2021) Vulnerability of cities to toxic airborne releases is written in their topology. *Scientific Reports* 11(1):23,029
- Fellini S, Marro M, Del Ponte AV, Barulli M, Soulhac L, Ridolfi L, Salizzoni P (2022) High resolution wind-tunnel investigation about the effect of street trees on pollutant concentration and street canyon ventilation. *Building and Environment* 226:109,763
- Fuka V, Xie ZT, Castro IP, Hayden P, Carpentieri M, Robins AG (2018) Scalar fluxes near a tall building in an aligned array of rectangular buildings. *Boundary-layer meteorology* 167:53–76
- Garbero V, Salizzoni P, Soulhac L (2010) Experimental study of pollutant dispersion within a network of streets. *Boundary-layer meteorology* 136:457–487

- Grimmond C, Oke TR (1999) Aerodynamic properties of urban areas derived from analysis of surface form. *Journal of Applied Meteorology and Climatology* 38(9):1262–1292
- Gromke C, Ruck B (2007) Influence of trees on the dispersion of pollutants in an urban street canyon – experimental investigation of the flow and concentration field. *Atmospheric Environment* 41(16):3287–3302
- Gromke C, Ruck B (2009) On the impact of trees on dispersion processes of traffic emissions in street canyons. *Boundary-Layer Meteorology* 131:19–34
- Gromke C, Ruck B (2012) Pollutant concentrations in street canyons of different aspect ratio with avenues of trees for various wind directions. *Boundary-Layer Meteorology* 144:41–64
- Guan D, Zhang Y, Zhu T (2003) A wind-tunnel study of windbreak drag. *Agricultural and forest meteorology* 118(1-2):75–84
- Hinze J (1967) Secondary currents in wall turbulence. *The Physics of Fluids* 10(9):122–125
- Huang YD, Hou RW, Liu ZY, Song Y, Cui PY, Kim CN, et al. (2019) Effects of wind direction on the airflow and pollutant dispersion inside a long street canyon. *Aerosol and Air Quality Research* 19(5):1152–1171
- Irwin H (1981) The design of spires for wind simulation. *Journal of wind engineering and industrial aerodynamics* 7(3):361–366
- Jeanjean AP, Hinchliffe G, McMullan W, Monks PS, Leigh RJ (2015) A CFD study on the effectiveness of trees to disperse road traffic emissions at a city scale. *Atmospheric Environment* 120:1–14
- Jeanjean AP, Buccolieri R, Eddy J, Monks PS, Leigh RJ (2017) Air quality affected by trees in real street canyons: The case of Marylebone neighbourhood in central london. *Urban Forestry & Urban Greening* 22:41–53
- Jia S, Wang Y (2021) Effect of heat mitigation strategies on thermal environment, thermal comfort, and walkability: A case study in Hong Kong. *Building and Environment* 201:107–988
- Kaimal JC, Wyngaard J, Izumi Y, Coté O (1972) Spectral characteristics of surface-layer turbulence. *Quarterly Journal of the Royal Meteorological Society* 98(417):563–589
- Krogstad PÅ, Antonia R (1999) Surface roughness effects in turbulent boundary layers. *Experiments in fluids* 27(5):450–460
- Kunadi AS, Silberstein RP, Thompson SE (2024) Variation in zero plane displacement and roughness length for momentum revisited. *Boundary-Layer Meteorology* 190(8):36
- Lin Y, Hang J, Yang H, Chen L, Chen G, Ling H, Sandberg M, Claesson L, Lam CKC (2021) Investigation of the reynolds number independence of cavity flow in 2D street canyons by wind tunnel experiments and numerical simulations. *Building and Environment* 201:107,965
- Linden J, Gustafsson M, Uddling J, Watne Å, Pleijel H (2023) Air pollution removal through deposition on urban vegetation: The importance of vegetation characteristics. *Urban Forestry & Urban Greening* 81:127–843
- Maison A, Flageul C, Carissimo B, Wang Y, Tuzet A, Sartelet K (2022) Parameterizing the aerodynamic effect of trees in street canyons for the street

- 985 network model MUNICH using the CFD model Code_Saturne. *Atmospheric*
 986 *Chemistry and Physics* 22(14):9369–9388
- 987 Majumdar D, Vita G, Ramponi R, Glover N, van Reeuwijk M (2024)
 988 The drag length is key to quantifying tree canopy drag. *arXiv preprint*
 989 *arXiv:241101570*
- 990 Manickathan L, Defraeye T, Allegrini J, Derome D, Carmeliet J (2018) Com-
 991 parative study of flow field and drag coefficient of model and small natural
 992 trees in a wind tunnel. *Urban forestry & urban greening* 35:230–239
- 993 Marro M, Gamel H, Méjean P, Correia H, Soulhac L, Salizzoni P (2020) High-
 994 frequency simultaneous measurements of velocity and concentration within
 995 turbulent flows in wind-tunnel experiments. *Experiments in Fluids* 61:1–13
- 996 Marucci D, Carpentieri M (2019) Effect of local and upwind stratification
 997 on flow and dispersion inside and above a bi-dimensional street canyon.
 998 *Building and Environment* 156:74–88
- 999 Montgomery DC, Peck EA, Vining GG (2021) Introduction to linear regression
 1000 analysis. John Wiley & Sons
- 1001 Nironi C, Salizzoni P, Marro M, Mejean P, Grosjean N, Soulhac L (2015) Dis-
 1002 persion of a passive scalar fluctuating plume in a turbulent boundary layer.
 1003 Part I: velocity and concentration measurements. *Boundary-layer meteorol-*
 1004 *ogy* 156:415–446
- 1005 Oke TR, Mills G, Christen A, Voogt JA (2017) *Urban climates*. Cambridge
 1006 University Press
- 1007 Peltola O, Aslan T, Aurela M, Lohila A, Mammarella I, Papale D, Thomas
 1008 CK, Vesala T, Laurila T (2025) Towards an enhanced metric for detecting
 1009 vertical flow decoupling in eddy covariance flux observations. *Agricultural*
 1010 *and Forest Meteorology* 362:110,326
- 1011 Poggi D, Porporato A, Ridolfi L, Albertson J, Katul G (2004) The effect of
 1012 vegetation density on canopy sub-layer turbulence. *Boundary-Layer Meteo-*
 1013 *rology* 111:565–587
- 1014 Raupach MR, Antonia RA, Rajagopalan S (1991) Rough-wall turbulent
 1015 boundary layers. *Applied Mechanics Reviews* 44:1–25
- 1016 Salem NB, Garbero V, Salizzoni P, Lamaison G, Soulhac L (2015) Mod-
 1017 elling pollutant dispersion in a street network. *Boundary-Layer Meteorology*
 1018 155:157–187
- 1019 Salizzoni P, Soulhac L, Mejean P, Perkins RJ (2008) Influence of a two-scale
 1020 surface roughness on a neutral turbulent boundary layer. *Boundary-layer*
 1021 *meteorology* 127(1):97–110
- 1022 Salizzoni P, Marro M, Soulhac L, Grosjean N, Perkins RJ (2011) Turbulent
 1023 transfer between street canyons and the overlying atmospheric boundary
 1024 layer. *Boundary-layer meteorology* 141(3):393–414
- 1025 Segura R, Krayenhoff ES, Martilli A, Badia A, Estruch C, Ventura S, Villalba
 1026 G (2022) How do street trees affect urban temperatures and radiation ex-
 1027 change? Observations and numerical evaluation in a highly compact city.
 1028 *Urban climate* 46:101–288
- 1029 Snyder WH (1972) Similarity criteria for the application of fluid models to the
 1030 study of air pollution meteorology. *Boundary-Layer Meteorology* 3(1):113–

- 1031 134
- 1032 Snyder WH, Castro IP (2002) The critical Reynolds number for rough-wall
1033 boundary layers. *Journal of wind engineering and industrial aerodynamics*
1034 90(1):41–54
- 1035 Soulhac L, Salizzoni P (2010) Dispersion in a street canyon for a wind direc-
1036 tion parallel to the street axis. *Journal of Wind Engineering and Industrial*
1037 *Aerodynamics* 98(12):903–910
- 1038 Soulhac L, Perkins RJ, Salizzoni P (2008) Flow in a street canyon for any
1039 external wind direction. *Boundary-Layer Meteorology* 126(3):365–388
- 1040 Soulhac L, Salizzoni P, Cierco FX, Perkins R (2011) The model SIRANE for
1041 atmospheric urban pollutant dispersion; part I, presentation of the model.
1042 *Atmospheric environment* 45(39):7379–7395
- 1043 Soulhac L, Salizzoni P, Mejean P, Perkins RJ (2013) Parametric laws to model
1044 urban pollutant dispersion with a street network approach. *Atmospheric*
1045 *Environment* 67:229–241
- 1046 Tennekes H, Lumley JL (1972) *A first course in turbulence*. MIT press
- 1047 Tomson M, Kumar P, Barwise Y, Perez P, Forehead H, French K, Morawska L,
1048 Watts JF (2021) Green infrastructure for air quality improvement in street
1049 canyons. *Environment international* 146:106–288
- 1050 Tritton DJ (2012) *Physical fluid dynamics*. Springer Science & Business Media
- 1051 Wang KX, Cui PY, Huang YD, Luo Y, Feng JJ, Wang JL, Xing GY (2024) Ef-
1052 fects of solar radiation and tree planting on photochemical reaction kinetics
1053 in urban street canyon. *Applied Thermal Engineering* 246:122–972
- 1054 Zhang L, Zhang Z, Feng C, Tian M, Gao Y (2021) Impact of various vegeta-
1055 tion configurations on traffic fine particle pollutants in a street canyon for
1056 different wind regimes. *Science of the Total Environment* 789:147–960
- 1057 Zhao Y, Chew LW, Fan Y, Gromke C, Hang J, Yu Y, Ricci A, Zhang Y, Xue
1058 Y, Fellini S, et al. (2023a) Fluid tunnel research for challenges of urban
1059 climate. *Urban Climate* 51:101–659
- 1060 Zhao Y, Li H, Bardhan R, Kubilay A, Li Q, Carmeliet J (2023b) The time-
1061 evolving impact of tree size on nighttime street canyon microclimate: Wind
1062 tunnel modeling of aerodynamic effects and heat removal. *Urban Climate*
1063 49:101–528